COO-1198-672

THE EFFECT OF POINT DEFECTS IN COPPER ON THE ANOMALOUS TRANSMISSION OF X-RAYS

Lewis Selig Edelheit

Department of Physics and Materials Research Laboratory

University of Illinois, Urbana, Illinois

February 1970

This is a technical information document based on a thesis submitted by Lewis Selig Edelheit in partial fulfillment of the requirements for the degree of Doctor of Philosophy in Physics in the Graduate College of the University of Illinois, 1970. The research was supported in part by the U. S. Atomic Energy Commission under Contract AT(11-1)-1198.

DISCLAIMER

COO-1198-672

THE EFFECT OF POINT DEFECTS IN COPPER ON THE ANOMALOUS TRANSMISSION OF X-RAYS

Lewis Selig Edelheit

Department of Physics and Materials Research Laboratory

University of Illinois, Urbana, Illinois

February 1970

This is a technical information document based on a thesis submitted by Lewis Selig Edelheit in partial fulfillment of the requirements for the degree of Doctor of Philosophy in Physics in the Graduate College of the University of Illinois, 1970. The research was supported in part by the U. S. Atomic Energy Commission under Contract AT(11-1)-1198.

THE EFFECT OF POINT DEFECTS IN COPPER ON THE ANOMALOUS TRANSMISSION OF X-RAYS

Lewis Selig Edelheit, Ph.D.
Department of Physics
University of Illinois, 1970

Anomalous X-ray transmission (Borrmann) measurements were made at 4.2 K on nearly perfect copper single crystals before and after irradiation at 20 K with 3 MeV electrons (total integrated flux 0.87×10^{18} electrons/cm^2). The intensity in the diffracted direction was measured for the (111), (222), (333), and (220) reflecting planes. The measured intensity changes were $1.15 \pm .4\%$, $4.52 \pm .6\%$, $8.90 \pm .8\%$, and $4.06 \pm .8\%$ respectively. A comparison of the observed intensity changes with theoretical predictions, assuming that the damage consists of isolated interstitials and vacancies, and using previously calculated displacements associated with these defects, indicates that the interstitial is not in the split (100) configuration. Possible configurations are the body centered interstitial or the split (111) interstitial.

Measurements after annealing at $80^\circ K$ and $300^\circ K$ were made. The measurements indicated that defect clusters were formed when the irradiated crystal was heated to $80^\circ K$, and some clusters remained after annealing at room temperature.

ACKNOWLEDGMENTS

The author gratefully acknowledges the constant advice and encouragement of Professor J. S. Koehler during the course of this investigation.

He also wishes to thank Dr. J. G. Ring and Dr. J. C. North for their patient instruction and assistance covering all aspects of this experiment. The author is indebted to Dr. F. W. Young, Jr., for the preparation of the samples and many helpful discussions.

The author acknowledges the award of a National Aeronautics and Space Administration Traineeship in Physics from September, 1965, to September, 1968, and a E. I. Du Pont de Nemours Fellowship from September, 1968, to June, 1969. This research was performed under a contract with the United States Atomic Energy Commission.

Finally, the author wishes to express his deep appreciation to his wife, Susan, for her patience, understanding, and encouragement during the course of this research.

TABLE OF CONTENTS

I. INTRODUCTION

Dynamical diffraction of X-rays is a powerful tool for investigating defects in nearly perfect crystals. Dislocations and large defect clusters can be photographed directly by means of X-ray transmission topography. Smaller defects can be investigated by integrated intensity measurements of anomalously transmitted X-rays (Borrmann effect). The clustering of oxygen in dislocation-free silicon[1] can reduce the anomalous X-ray transmission by two orders of magnitude. Efimov et al.[2] and Maruyama[3] have investigated the effects of impurities and vacancies in germanium on Borrmann intensities. Defect clusters produced in germanium and silicon by fast neutron bombardment attenuate the anomalously transmitted intensity.[4,5] In copper, Baldwin et al.[6] found that changes in Borrmann intensities of several orders of magnitude resulted from irradiation with $4 \times 10^{19}/cm^2$ fast neutrons. Recently, Batterman[7] has determined the position occupied by impurity atoms in a silicon lattice by measuring the X-ray fluorescence of the impurity during a dynamical diffraction process.

The present experiment was undertaken to determine the geometrical nature of a copper interstitial in a copper lattice. The previous measurements made in order to study single interstitials in copper have primarily been low temperature measurements of resistivity and stored energy.[8] These determine the existence of the defect, but do not give much information about the microscopic configuration of the interstitial. Several models of this configuration have been proposed.[9-14] In these models the point atoms interact with two body forces. A computer

calculation then minimizes the energy associated with the various configurations. In the models, the coordinates of the atoms near the defect are considered explicitly, while the remainder of the crystal is treated as an elastic continuum which is appropriately joined to the discrete atomic arrangement used near the interstitial. The various calculations agree in that the split (100) interstitial has the smallest formation energy and is, therefore, the most stable. Some of the calculations, however, indicate that the formation energies of four or five contending configurations lie within 10% of the split (100) value. The variations in the calculated energies can be that large, depending upon the form and hardness of the interatomic potential chosen and the number of atoms which are treated as individual particles in the calculations. Furthermore, the calculations do not take into account the electron redistribution in a very realistic manner. In addition, any possible influence of d electron redistribution is neglected in all calculations.

Anomalous X-ray transmitted intensity is very sensitive to the position of an atom in the unit cell, and thus can be used to experimentally determine the configuration of the interstitial and its surrounding atoms. In addition, contrary to electrical resistivity measurements, anomalous transmission is very sensitive to the clustering of interstitials and thus can yield much information concerning the annealing processes in copper.

II. DESCRIPTION OF WAVE FIELDS

Anomalous transmission of X-rays was first observed by Borrmann,[15] who noted that the apparent absorption coefficient of X-rays in crystals is greatly reduced for X-rays incident at the Bragg angle. The theory of the diffraction of X-rays through thick, absorbing, perfect crystals has been reviewed by several authors.[16,17] The configuration is shown in Figure 1. A plane wave is incident on the crystal at the Bragg angle, θ_B, as shown. The "two beam" case is assumed where the only other wave excited in the crystal is in a single diffracted direction. The total electric field inside the crystal is then the sum of the two coherent plane waves:

$$\underset{\sim}{E}(\underset{\sim}{r},t) = \underset{\sim}{E}_o \, e^{i(\omega t - \underset{\sim}{K}_o \cdot \underset{\sim}{r})} + \underset{\sim}{E}_H \, e^{i(\omega t - \underset{\sim}{K}_H \cdot \underset{\sim}{r})} , \qquad (1)$$

where $\underset{\sim}{E}_o$ and $\underset{\sim}{E}_H$ are the electric field vectors of the incident and diffracted waves respectively, and $\underset{\sim}{K}_o$ and $\underset{\sim}{K}_H$ are the incident and diffracted wave vectors. The wave vectors satisfy the Bragg condition $\underset{\sim}{K}_o - \underset{\sim}{K}_H = \underset{\sim}{h}$, where $\underset{\sim}{h}$ is the reciprocal lattice vector for the diffracting planes in question:

$$\underset{\sim}{h} = \frac{4\pi}{\lambda} \underset{\sim}{n} \sin \theta_B , \qquad (2)$$

where

$$\underset{\sim}{n} = \frac{h\underset{\sim}{i} + k\underset{\sim}{j} + l\underset{\sim}{z}}{\sqrt{h^2 + k^2 + l^2}} \qquad (3)$$

is the unit normal to the (hkl) planes.

These two waves add together to form a traveling wave moving in the direction of the bisector of the angle between $\underset{\sim}{K}_o$ and $\underset{\sim}{K}_H$ (i.e.

Figure 1. Geometry of the beams when anomalous transmission is occuring. When the beam emerges from the back face, it splits into two beams, one in the forward direction, and one in the diffracted direction. The energy in the beam flows along the atomic planes in the crystal.

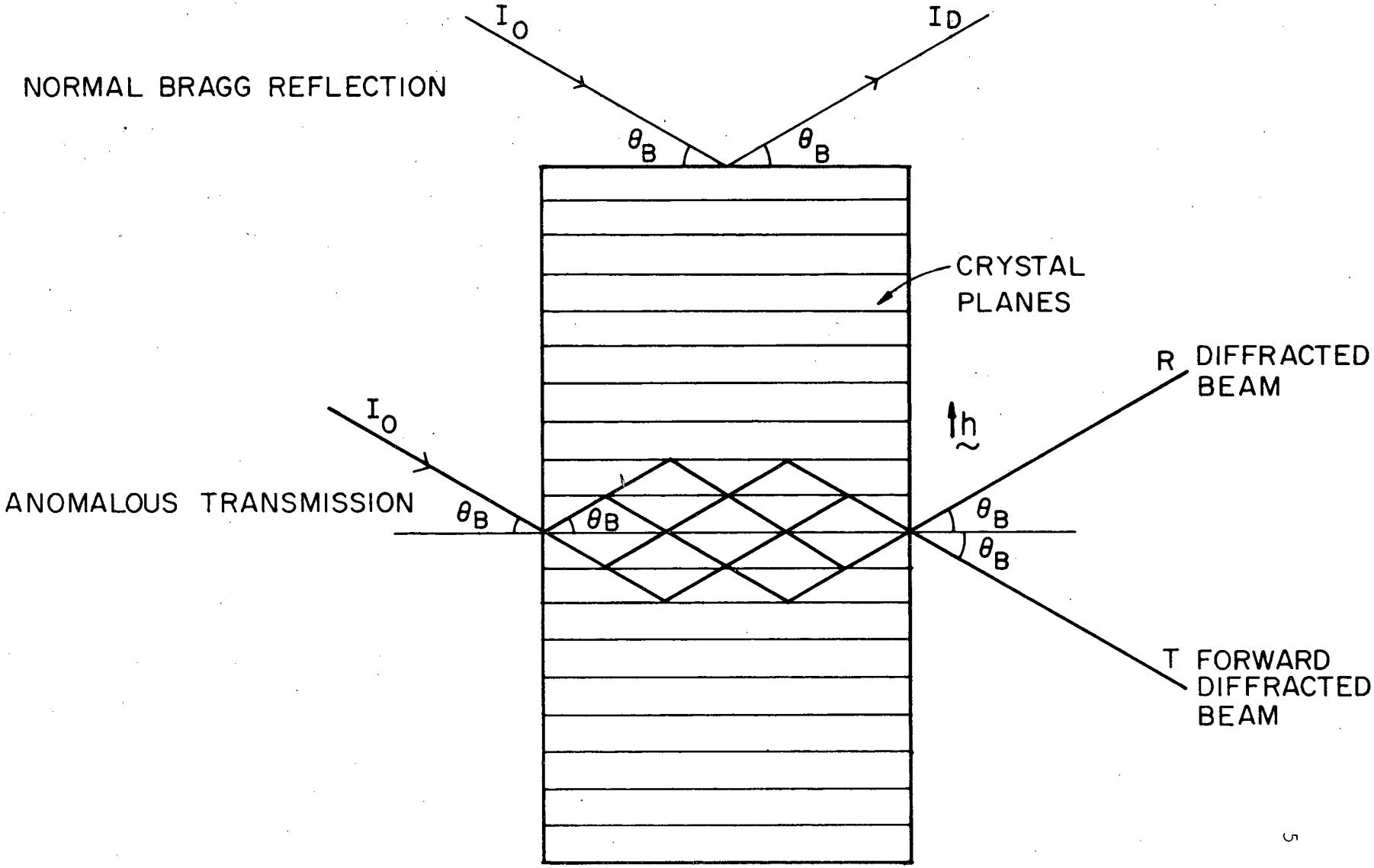
NORMAL BRAGG REFLECTION
I_O
I_D
θ_B
θ_B
CRYSTAL PLANES
R DIFFRACTED BEAM
$\underset{\sim}{h}$
I_O
ANOMALOUS TRANSMISSION
θ_B
θ_B
θ_B
θ_B
T FORWARD DIFFRACTED BEAM

in a direction parallel to the diffracting planes) and a standing wave at right angles to this direction.

The time averaged field intensity, $\frac{1}{2}\underset{\sim}{E}\underset{\sim}{E}^*$ is

$$\tfrac{1}{2}|\underset{\sim}{E}|^2 = \tfrac{1}{2}[\,|\underset{\sim}{E}_o|^2 + |\underset{\sim}{E}_H|^2 + 2\underset{\sim}{E}_o \cdot \underset{\sim}{E}_H \cos(\underset{\sim}{h}\cdot\underset{\sim}{r})\,] \quad . \tag{4}$$

In anomalous transmission $|\underset{\sim}{E}_o| = |\underset{\sim}{E}_H|$ and the intensity becomes

$$\tfrac{1}{2}|E|^2 = |\underset{\sim}{E}_o|^2(1 \pm P\cos(\underset{\sim}{h}\cdot\underset{\sim}{r}) \tag{5}$$

where $\underset{\sim}{E}_o \cdot \underset{\sim}{E}_H = P|\underset{\sim}{E}_o|^2$, and where P = 1 if the incident electric field is polarized perpendicular to the incident direction (σ polarization) and $P = \cos 2\theta_B$ if the field is polarized in the plane of incidence (π polarization). For both states of polarization, the Poynting's vector $\underset{\sim}{E} \times \underset{\sim}{H}^*$ gives an average energy flow along the atomic planes. The ($\pm$) sign takes into account the two cases in which the two plane waves have relative phases of zero or π. The branch with the minus sign is called the α branch; the branch with the plus sign is the β branch.

The expression for the field intensity shows why anomalous transmission can occur. The photoelectric absorption of an atom is proportional to the electric field intensity at the atom. If the nodal planes of the electric field ($\underset{\sim}{h}\cdot\underset{\sim}{r} = 2n\pi$) are coincident with the atoms which make up the diffracting planes, much smaller than normal absorption takes place. Figure 2 is a schematic representation of the distribution of electric field intensity for the four cases described by (5). It is apparent that only the σ polarization of the α branch has nodal planes at the atomic sites. In a thick crystal this is the only beam

Figure 2. Possible configuration of the standing wave patterns assuming that the nodes of the α pattern, σ polarization, coincide with the atomic planes, (a) α branch, σ polarization (b) β branch, σ polarization (c) α branch π state (d) β branch, π state.

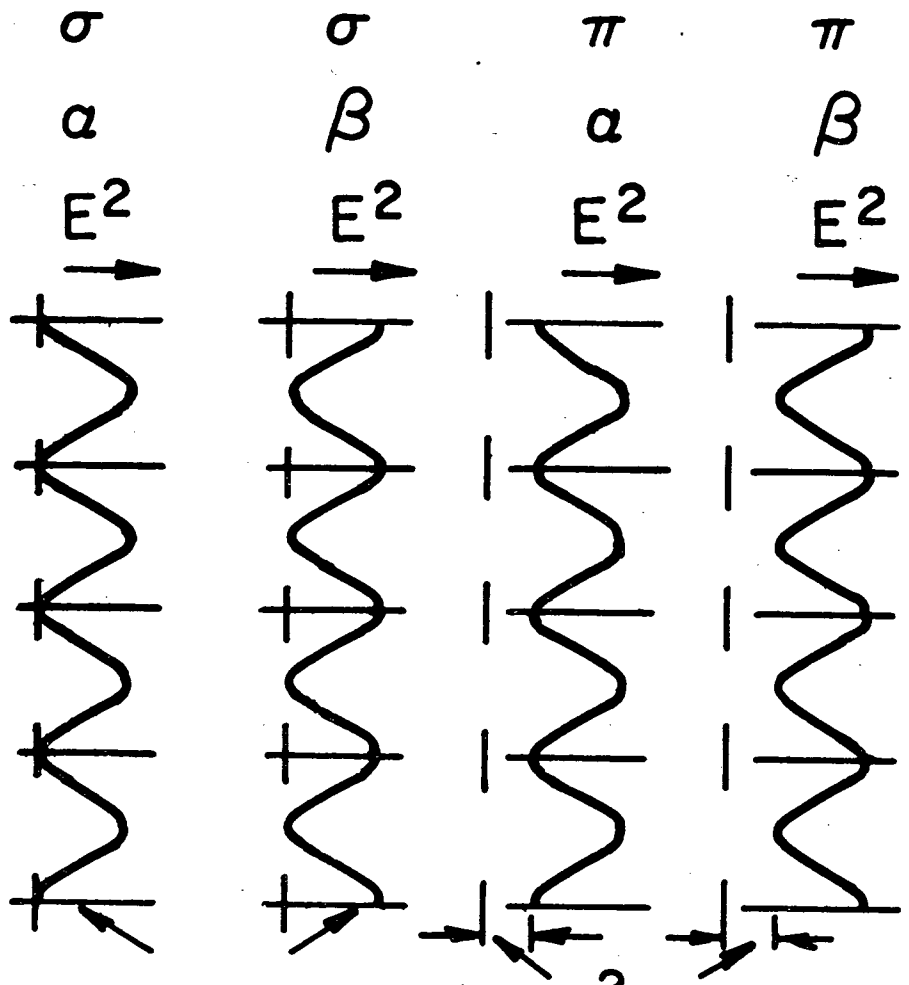
σ
α
E²
σ
β
E²
π
α
E²
π
β
E²
ATOMIC PLANES
E²(1-P)
(a)
(b)
(c)
(d)

which emerges from the back face of the crystal, and, therefore, we need only consider the case:

$$\tfrac{1}{2}|\underset{\sim}{E}|^2 = |\underset{\sim}{E}_o|^2(1-\cos(\underset{\sim}{h}\cdot\underset{\sim}{r})) = |\underset{\sim}{E}_o|^2[1-\cos(\frac{2n\pi y}{d_{hkl}})] , \qquad (6)$$

where n is the order of reflection, d_{hkl} is the distance between the crystal planes, and y is a coordinate perpendicular to the crystal planes (y = 0 is at a particular crystal plane, y = d_{hkl} at the next plane, etc.).

We now consider the effect of photoelectric absorption. For X-rays incident on a crystal at an angle, θ, not satisfying Bragg's law, the intensity emerging from a crystal of thickness t is given by:

$$I(t) = I_o \exp - \frac{\mu_o t}{\cos\theta} , \qquad (7)$$

where $\mu_o = \sigma_o N_o$ is the linear absorption coefficient, σ_o is the photoelectric cross section, and N_o is the number of atoms per unit volume. It is assumed that the only important absorbing process is photoelectric absorption. For the crystals used in the case of anomalous transmission, σ_o must be replaced by[16]

$$\sigma^* = \sigma_o(1-\epsilon_h) \qquad (8)$$

where

$$\epsilon_h = \frac{f''_{hkl}(\theta_B)}{f''_o(\theta_B)} \qquad (9)$$

is the ratio of the imaginary part of the scattering amplitude in the (hkl) direction to that of the imaginary part of the forward scattering amplitude. It has been shown that[18-20]

$$\epsilon_h = \epsilon_{oh}\, e^{-M} \qquad (9a)$$

where $\epsilon_{oh} \cong 1$ and M is the Debye-Waller factor. At 4.2°K, $e^{-M} \cong 1$, and thus $\sigma^* \cong 0$. Therefore, the absorption coefficient is very small as expected. ϵ_h has been determined experimentally for several materials and wavelengths. Also, Wagenfeld[20] has made quantum-mechanical calculations of the value of ϵ_{oh}.

We give here a semiquantitative argument to show the effect of displaced atoms on the anomalous transmission. The geometry is shown in Figure 3. Let $\underset{\sim}{r}_o$ be the position of the center of an atom from the origin. Let $\underset{\sim}{r}$ be the position of a volume element dv of the atom, and $\underset{\sim}{r}_a$ be the distance from the center of the atom to the volume element. Assume that $\sigma(\underset{\sim}{r}_a)dv$ is the contribution to the average photoelectric absorption by the volume element dv, i.e.

$$\sigma_o = \int_v \sigma(r_a)dv \ . \tag{10}$$

Since σ^* is proportional to the intensity $|\underset{\sim}{E}|^2$, we have that the cross section of the atom at $\underset{\sim}{r}_o$ is given by

$$\sigma^*(r_o) = K \int_v |\underset{\sim}{E}|^2 \, \sigma(\underset{\sim}{r}_a)dv \tag{11}$$

where K is a proportionality constant. We assume that the absorption from the atom at $\underset{\sim}{r}_o$ does not distort the shape of the intensity $|E|^2$. This is a good assumption for all atoms and clusters whose dimensions are much smaller than an extinction length (≈ 1 micron). Thus:

$$\sigma^*(\underset{\sim}{r}_o) = K \int (1-\cos(\underset{\sim}{h}\cdot\underset{\sim}{r}))\sigma(\underset{\sim}{r}_a)dv$$

$$= K \int (1-\cos[\underset{\sim}{h}\cdot(\underset{\sim}{r}_o+\underset{\sim}{r}_a)])\sigma(r_a)dv \ . \tag{12}$$

Figure 3. Geometry used to calculate the absorption of an atom in a standing wave pattern. As can be seen, the absorption by the atom depends greatly on the order of reflection.

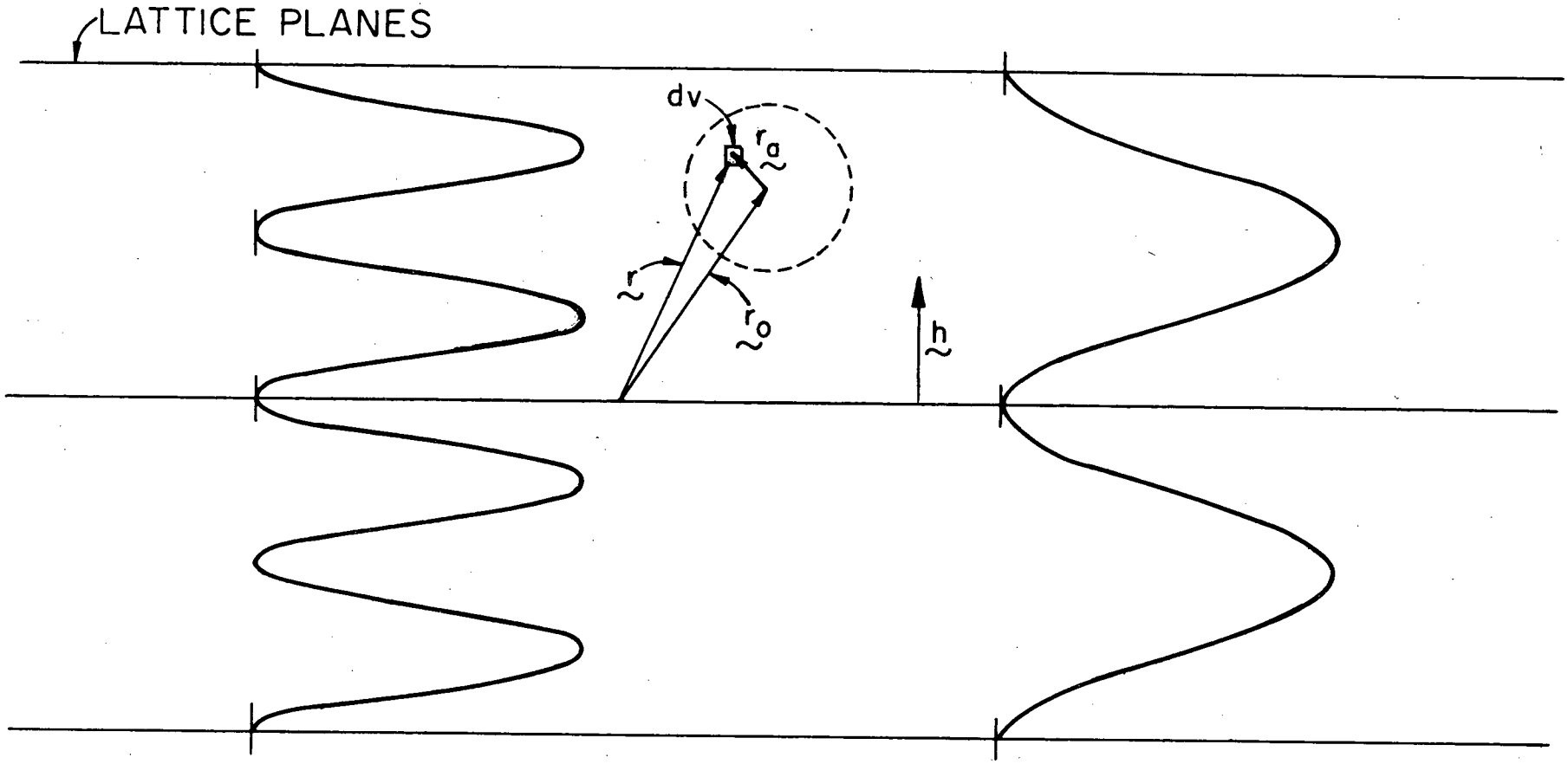

$\rightarrow |E|^2$ 2nd. order n=2

$\rightarrow |E|^2$ 1st. order n=1

We expand the cosine function noting that if $\sigma(\underset{\sim}{r}_a) = \sigma(-\underset{\sim}{r}_a)$, the term containing $\sin(\underset{\sim}{h}\cdot\underset{\sim}{r}_o)$ vanishes and we get

$$\sigma^*(\underset{\sim}{r}_o) = K\sigma_o - k\cos(\underset{\sim}{h}\cdot\underset{\sim}{r}_o)\int \cos(\underset{\sim}{h}\cdot\underset{\sim}{r}_a)\sigma(\underset{\sim}{r}_a)dv$$

$$= K\sigma_o\left[\left(1 - \frac{\cos(\underset{\sim}{h}\cdot\underset{\sim}{r}_o)}{\sigma_o}\int \cos(\underset{\sim}{h}\cdot\underset{\sim}{r}_a)\sigma(\underset{\sim}{r}_a)dv\right]. \qquad (13)$$

The average of $\sigma(\underset{\sim}{r}_o)$ over all positions in the field gives the average cross section and, therefore, K = 1. We also note that if $\underset{\sim}{h}\cdot\underset{\sim}{r}_o = 2n\pi$, i.e. the atom is at a lattice site:

$$\sigma_h^*(0) = \sigma_o\left(1 - \frac{\int \cos(\underset{\sim}{h}\cdot\underset{\sim}{r}_a)\sigma(\underset{\sim}{r}_a)dv}{\sigma_o}\right). \qquad (14)$$

Thus if we compare this equation with Eq. (8), we see that for this calculation,

$$\epsilon_h = \frac{\int \cos(\underset{\sim}{h}\cdot\underset{\sim}{r}_a)\sigma(\underset{\sim}{r}_a)dv}{\sigma_o} \qquad (15)$$

is related to the weighted distribution of absorbing power within the atom. We now have that the effective cross section for absorption of an atom at $\underset{\sim}{r}_o$ is given by

$$\sigma_h^*(\underset{\sim}{r}_o) = \sigma_o(1 - \epsilon_h\cos(\underset{\sim}{h}\cdot\underset{\sim}{r}_o)) \quad . \qquad (16)$$

If an atom at a lattice site is displaced from a lattice site to a position $\underset{\sim}{r}_o$ in the unit cell the change in the effective cross section is

$$\Delta\sigma_h^*(\underset{\sim}{r}_o) = \sigma_o[1 - \epsilon_h\cos(\underset{\sim}{h}\cdot\underset{\sim}{r}_o)] - \sigma_o[1 - \epsilon_h\cos(2n\pi)]$$

$$= \sigma_o\epsilon_h(1 - \cos(\underset{\sim}{h}\cdot\underset{\sim}{r}_o)) \quad . \qquad (17)$$

To get the net change in the anomalous transmission due to an interstitial-vacancy pair, we must also consider the atoms around the interstitial and vacancy which are displaced from their lattice sites. If we assume that the interstitials are randomly distributed in the lattice, and that the displacement of a lattice atom is due to a single interstitial we obtain

$$\Delta\sigma^*_{h\ net} = \sigma_o \epsilon_h \sum_j (1 - \cos(\underset{\sim}{h}\cdot\underset{\sim}{r}_{oj})) \tag{18}$$

where the sum is over all atoms that have been displaced by a single interstitial-vacancy pair (including the interstitial atom itself). We now have an additional absorption coefficient

$$\mu^* = \Delta\sigma_h^*{}_{net}\ N_i\ , \tag{19}$$

where N_i is the number of interstitials per unit volume. If $C_i = \frac{N_i}{N_o}$ is the concentration of interstitials, we have

$$\mu^* = \mu_o \epsilon_h C_i \sum_j (1 - \cos(\underset{\sim}{h}\cdot\underset{\sim}{r}_{oj}))\ . \tag{20}$$

The fractional attenuation of the transmitted intensity due to these defects is

$$\begin{aligned}\frac{\Delta I}{I} &= (e^{-\mu^* t^*} - 1) \\ &\cong \frac{\mu_o t}{\cos\theta_B} \epsilon_h C_i \sum_j (1 - \cos(\underset{\sim}{h}\cdot\underset{\sim}{r}_{oj}))\end{aligned} \tag{21}$$

where $t^* = \frac{t}{\cos\theta_B}$ is the effective thickness of the crystal at the Bragg angle. The expansion is good for small concentrations of interstitials.

It is apparent that anomalous transmission is sensitive to the displacements $\underset{\sim}{r}_{oj}$. If we consider the expression $\cos(\underset{\sim}{h}\cdot\underset{\sim}{r}_{oj}) = \cos(\frac{2n\pi y}{d_{hkl}})$, we see that for an atom halfway between the planes $(1 - \cos(\frac{2n\pi y}{d_{hkl}}))$ equals two for the first order reflection (n = 1), and zero for the second order reflection (n = 2). This is shown in Figure 3. Thus for a "body centered" interstitial the absorption in the first order is much larger than in the second order.

In gold[21] and silver,[22] Shimomura has shown that after electron irradiation at 130°K one sees interstitial loops by electron microscopy done below Stage III. He finds that the clusters become smaller as one anneals through Stage III. Recently, Scheidler and Roth[23] have shown by electron microscopy that clusters exist at 300°K in copper irradiated at 15°K. This suggests that one should examine the effect of clustering on the absorption. If we assume a concentration C_1 of independent clusters whose size is small compared to an extinction length, the previous arguments are the same and give

$$\left.\frac{\Delta I}{I}\right|_1 = \frac{\mu_o t}{\cos\theta_B} \epsilon_h C_1 \sum_j (1 - \cos(\underset{\sim}{h}\cdot\underset{\sim}{r}_{oj1})) \quad . \tag{22}$$

This problem has been treated by Dederichs,[24,25] and by Young, Baldwin, and Dederichs.[26] Shimomura's work suggests that the clusters are in the form of dislocation loops. From continuum theory, the displacement field for an isotropic elastic solid in the asymptotic region is given by

$$r_{oj1}(r) = \frac{b R_o^2}{8r^2} \frac{1-2\nu}{1-\nu} (2\underset{\sim}{b}^o(\underset{\sim}{b}^o\cdot\underset{\sim}{e})-\underset{\sim}{e}) + \frac{3}{1-\nu} \underset{\sim}{e}(\underset{\sim}{b}^o\cdot\underset{\sim}{e})^2 \tag{23}$$

with $\underset{\sim}{b}^o = \frac{\underset{\sim}{b}}{|\underset{\sim}{b}|}$, $\underset{\sim}{e} = \frac{\underset{\sim}{r}}{|\underset{\sim}{r}|}$, and ν is Poisson's ratio ($\cong 1/3$ for copper). πR_o^2 is the surface area of the loop, $\underset{\sim}{b}$ is the Burgers vector (perpendicular to the loop plane), and the volume of the loop is

$$V = b\pi R_o^2 \cong \pi R_o^2 d_{hkl} . \tag{24}$$

In order to evaluate the expression

$$\sum_j (1 - \cos(\underset{\sim}{h}\cdot\underset{\sim}{r}_{ojl})) \cong \int \frac{dr}{V_c}\{1 - \cos[\underset{\sim}{h}\cdot\underset{\sim}{r}_{ojl}(\underset{\sim}{r})]\} \tag{25}$$

($V_c = \frac{a^3}{4}$ is the volume of the unit cell), one can show[25,26] that if we replace $\underset{\sim}{r}_{ojl}(\underset{\sim}{r})$ by the asymptotic expression, the value of the sum is approximately given by

$$\sum_j (1 - \cos(\underset{\sim}{h}\cdot\underset{\sim}{r}_{ojl})) \approx \frac{R_o^3}{V_c}\frac{(hb)^{3/2}}{2} \tag{26}$$

and, therefore,

$$\frac{\Delta I}{I} \approx \frac{\mu_o t \epsilon_h C_1 R_o^3 (bh)^{3/2}}{2V_c \cos\theta_B} . \tag{27}$$

This is a much larger change than an equivalent number of randomly distributed point defects. If the concentration of interstitials is C_i and if the clusters are loops on the (111) planes, than the number of atoms in the cluster is

$$n_1 = 4\pi R_o^2 \frac{a}{\sqrt{3}}\frac{4}{a^3} = 7.24\frac{R_o^2}{a^2} \tag{28}$$

where $a = 3.61$ Å in copper. We then have

$$C_1 = \frac{1.8C_i}{R_o^2} \tag{29}$$

and, therefore, for a given crystal reflection

$$\frac{\Delta I}{I} \propto C_1 R_o^3 \propto C_i R_o \quad . \tag{30}$$

Therefore, for a given number of interstitial atoms, the change in intensity is proportional to the radius of the clusters into which the interstitials are formed.

Dederichs[24-26] treats the entire problem of the effect of point defects on anomalous transmission by considering the scattering to be from an effective optical potential. He develops a generalized Debye-Waller function including the displacements due to defects as well as due to thermal vibrations.

This treatment leads to the same result as in Eq. (21). He also considers the effect of diffuse scattering by defects in which the scattered X-ray does not satisfy Bragg's condition and is, therefore, absorbed by the crystal. The diffuse scattering is wavelength dependent and is very sensitive to the clustering of defects. He finds[25] that for MoKα X-rays this is a small effect if the clusters present in election irradiated copper are not too large. Therefore, the diffuse scattering will not be considered in our calculations.

III. EXPERIMENTAL PROCEDURE

A. Sample Preparation

Single crystals of 99.999+% copper were prepared for Borrmann X-ray studies by Dr. F. W. Young, Jr., at the Oak Ridge National Laboratory. This preparation has been described previously.[27] A 1 × 1 × 2 cm parallelopiped was cut from the crystal by an acid saw technique.[28] This crystal was annealed at 1075°C for about two weeks to eliminate dislocations. The crystal was then irradiated with 10^{17} nvt fast neutrons at a temperature below 100°C in order to pin the remaining dislocations and thus minimize damage due to handling. It has been shown[29] that the effect on the anomalous transmission due to this irradiation is small and it is assumed that the effect remains a constant during the experiment. After irradiation, the crystal was sliced into 1 × 1 × t cm pieces (t between .025 and .205). For our experiment two adjacent slices were chosen. The two crystals had (110) faces to within 0.5°. They were polished and electropolished[28] to eliminate surface damage.

The thickness of the crystals was determined by absolute integrated intensity measurements, and also by the relative intensities of various orders of reflection. The crystal to be irradiated had a thickness of 0.9 ± 0.1 mm while the other crystal was 0.8 ± 0.1 mm thick. Due to the polishing process, the crystal faces were slightly convex. Thus, the crystal was thicker at the center than near the faces. This variation in thickness with position had two effects. First, since we were interested in the change in X-ray intensity due to irradiation, any

change in intensity due to thickness variations had to be minimized. In addition, it can be shown[30,31] that the change in intensity due to slowly varying strains introduced into the crystal depends on the angle that the diffracting planes make with the surface of the crystal, which in turn partly depends on the curvature of the surface.

X-ray topographs were taken and are shown in Figure 4. There are a few dislocations in the corners of the crystals, but there are none in the central region where the intensity measurements were made.

Although the presence of neutron irradiation damage permitted handling of the crystals, Hunter,[32] Penning and Polder,[30,31] and others have shown that strains of very small magnitude can be detected by anomalous transmission. Since the measurements were made at very low temperatures, mechanical strains due to differential thermal contractions could have reduced the diffracted X-ray intensity drastically if the crystals were rigidly supported. Thus the crystals were placed in a copper holder as shown in Figures 6 and 7. There was approximately .005" clearance on all sides, and thus the only external force on the crystals was due to gravity. Thin (.005") Be-Cu strips prevented the crystals from falling out of the mount.

B. Cryostat

Single crystal X-ray diffractometers usually have a fixed X-ray tube and beam collimator and require a two circle goniometer to orient the cryostat specimen. This requirement is accentuated when the crystal must be kept at low temperatures. In a cryostat designed to cool a single crystal to very low temperatures, the entire goniometer may be

Figure 4. MoKα X-ray topograph of the two copper crystals used in the experiment. The reflecting planes are (111).

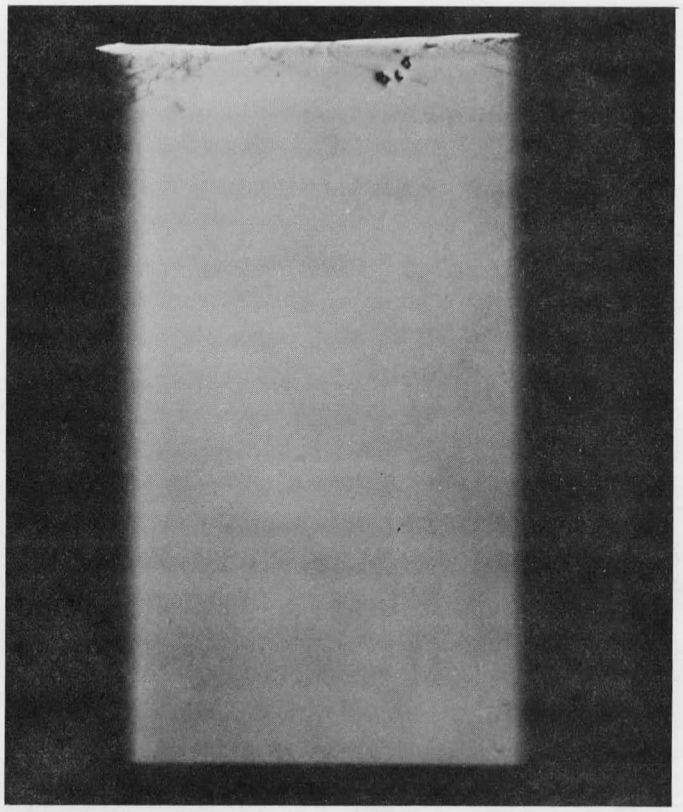

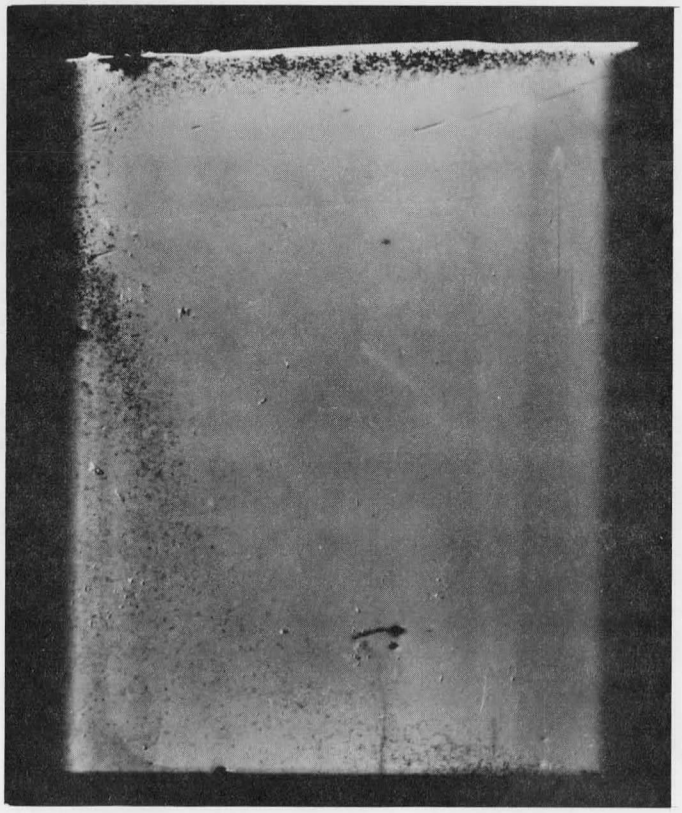

located within the cryostat, or the entire cryostat may be placed upon a large goniometer. The main advantages of the former approach are that small and easily constructed goniometers are suitable, and that the cryostat permanently retains its original position. The disadvantages are that manipulation of the goniometer must be by remote control, making precise orientation difficult; that the control rods must pass through the liquid helium chamber or vacuum chamber, with increased consumption of liquid helium; and also that the low temperature of the goniometer may result in faulty operation. In the second approach, the advantages are intact vacuum and liquid helium chambers and ample precision in orientation. The main disadvantage is that tilting the cryostat through large angles may cause sufficient internal movement to result in loss of thermal insulation. One possible approach is to construct the X-ray system, including the X-ray tube, on a massive 2 or 3 circle goniometer.[33]

In the experiment described here, one circle of the goniometer is located inside the cryostat, and the cryostat, in turn, is placed upon the other circle of the goniometer. This eliminates many of the disadvantages of the two systems.

The basic liquid helium cryostat, Figure 5, is a 5 liter dewar purchased from the Superior Air Products Company, Newark, New Jersey. A rigid support for the tail of the liquid helium reservoir was achieved by the use of two concentric nylon cylinders which provide thermal insulation as well as physical support. The entire rigid tail assembly, including the liquid nitrogen shield, was supported by a .010" thick stainless steel cylinder. The X-ray windows, epoxied to the outer can,

Figure 5. Helium cryostat: a) dewar mounting flange; b) 12 liter capacity liquid nitrogen reservoir; c) 5 liter liquid helium reservoir; d) external control of bead chain in order to adjust ϕ rotation; e) 7 liter liquid nitrogen reservoir surrounding the tail section of the helium reservoir; f) .010" stainless steel cylinder supporting rigid tail section; g) 2 concentric nylon cylinders for mechanical support and thermal insulation of rigid tail; h) external chamber wall (not in section); j) valve opening to van de Graaff when irradiating; k) .002" aluminum coated Mylar X-ray windows.

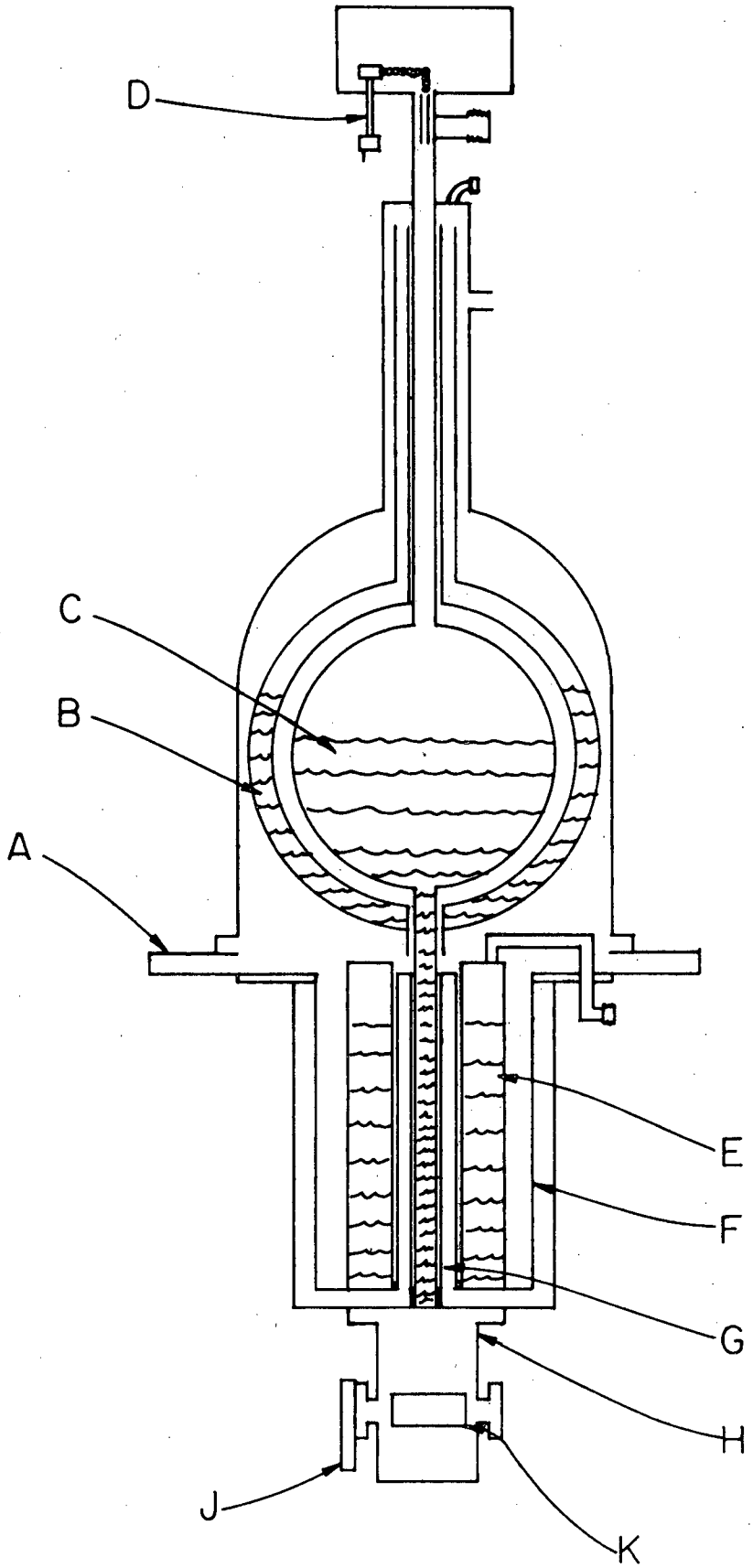
D
C
B
A
E
F
G
H
J
K

were .002" aluminum coated mylar windows donated by the Standard Packaging Company. Each window was 1-1/8" high and subtended an angle of 120°. The windows could support one atmosphere of pressure, however, the X-ray attenuation was negligible.

The outer can could be rotated on a ball bearing allowing the vacuum valve, which can be fastened to the van de Graaff generator, to be positioned in front of the samples.

The irradiation windows on the specimen chamber, Figure 6, were .0015" Alcoa 2024-F "Duraluminium" windows. Mylar is damaged by electron irradiation and thus could not be used. These windows could also support one atmosphere of pressure. They were also 1-1/8" high and subtended 120°.

The samples were cooled by helium gas. Liquid helium flowed into the chamber by means of a tube from the reservoir. The rate of helium flow could be adjusted by a valve similar to that designed by Whitehouse,[34] et al. The helium exchange gas was cooled by copper fins attached to this tube. A 3/16" thick copper shield allowed the upper crystal to be irradiated but protected the lower crystal from electrons. The shield could be lowered to clear access to the lower crystal for the X-ray measurements. The sample could be heated by means of a 200Ω insulated wire wrapped around the sample chamber.

One circle of the goniometer was entirely within the cryostat. The sample mount was attached to a worm wheel. The worm wheel was, in turn, attached to a bearing (Figure 7) which allowed the crystal to rotate freely. The worm wheel was turned by a worm gear, which was

Figure 6. Sectional view of the specimen chamber: a) copper crystals to be measured; b) $\frac{1}{4}$" brass aperture for electron beam; c) valve to van de Graaff; d) ball bearing race to rotate outer chamber; e) .010" wall inconel tubes conducting liquid helium to sample chamber; f) liquid nitrogen temperature radiation shield; g) 3/32" diameter stainless steel bead chain wrapped around a sprocket; h) worm gear; i) Barden SFR1-4R Bearing (only one shown); j) "Xactglo" heating element to vary sample temperature; k) worm wheel for Φ rotation; l) cut outs in sample mount used to locate the crystal position; m) copper posts used to align the electron beam with respect to the sample; n) 3/16" copper shield which can be raised from above to shield the lower copper crystal from electron irradiation; o) copper fins used to cool helium exchange gas.

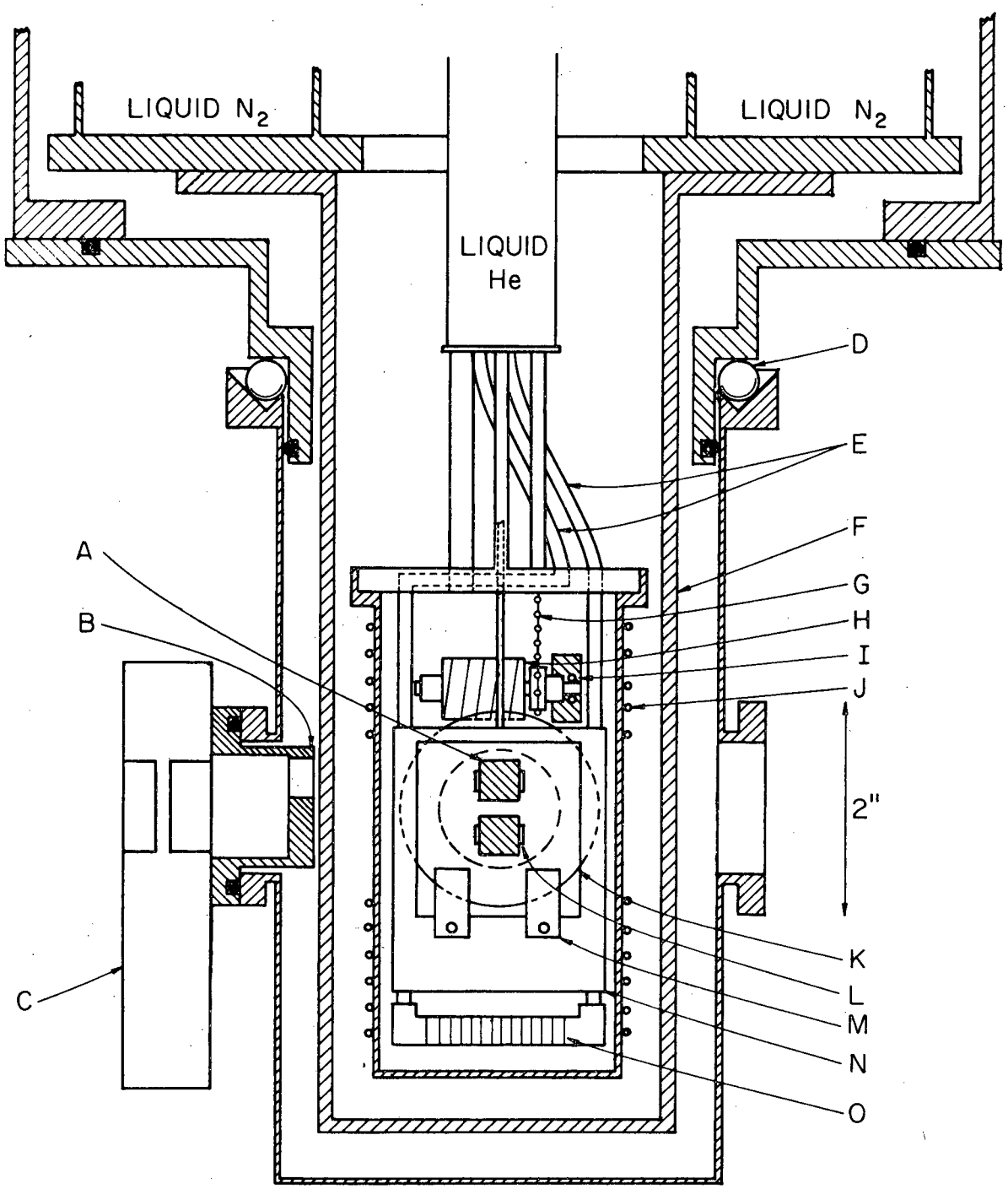
LIQUID N_2
LIQUID N_2
LIQUID
He
D
E
F
G
H
I
J
A
B
2"
C
K
L
M
N
O

Figure 7. Rotating sample holder: a) copper crystals which are free to move in the mount; b) 1/16" thick copper mount; c) .005" Be-Cu strip to prevent sample from falling out; d) worm wheel which is turned by the worm gear (e); f) inner bearing clamp; g) Miniature Precision Bearing Company 3TK1 bearing with stainless steel race and balls with teflon spacer slugs; h) outer bearing clamp.

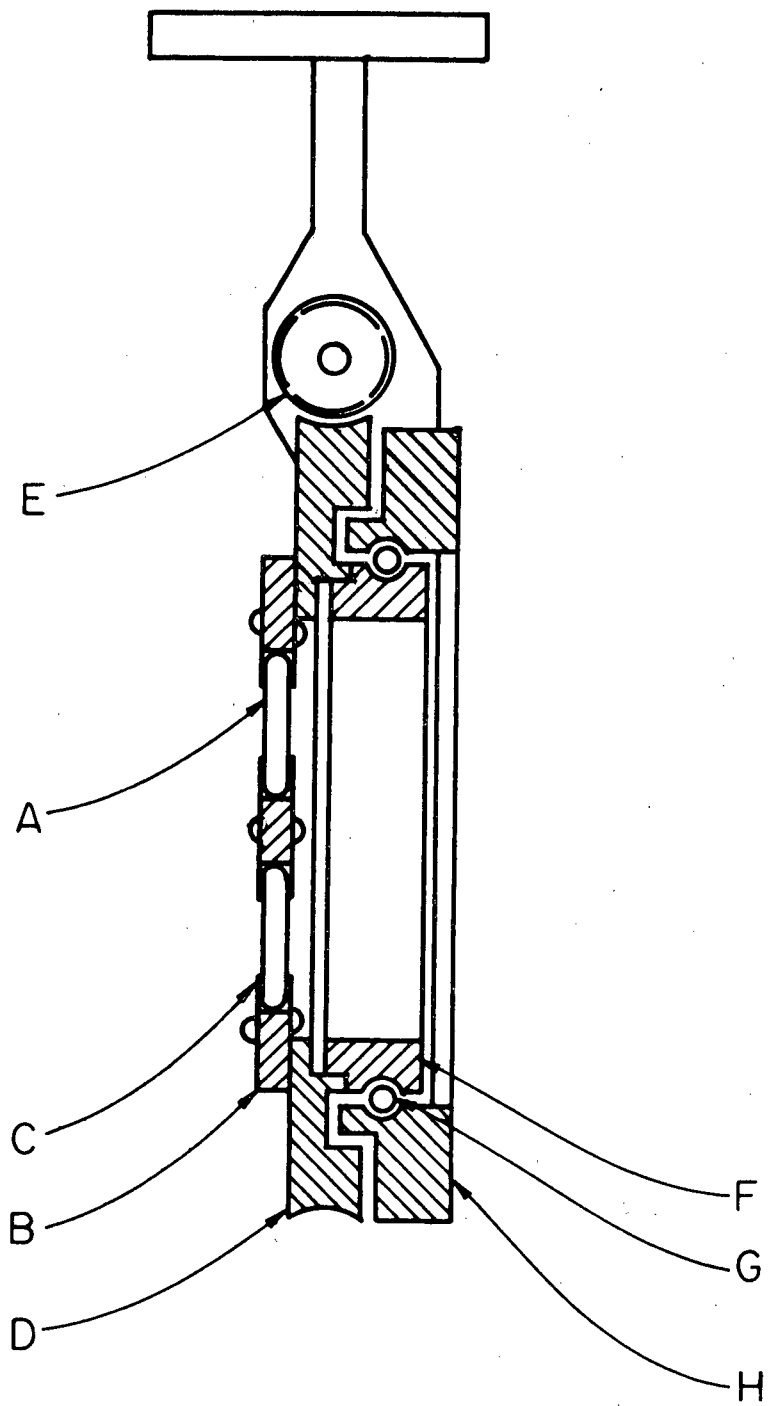
E
A
C
B
D
F
G
H

turned by a stainless steel bead chain from above. The tension in the bead chain could be adjusted by a spring pulley (not shown) at the top of the cryostat. In this way, the sample could be rotated 360°, about the normal to the crystal face. This angle will be referred to as ϕ.

The thermal loss of the entire cryostat was less than two liters of liquid helium per 24 hours. The sample temperature was measured by means of a carbon resistor and all X-ray measurements were made below 4.5°K.

C. X-Ray Apparatus

Figure 8 is a schematic diagram of the X-ray system in operation. The cryostat is placed on a 1" aluminum plate which, in turn, is placed upon two orthogonally constructed sets of 1.5" diameter steel rods and linear ball bushings which provide horizontal (x and y) motion with respect to the X-ray beam. The entire cryostat can be removed from this X-ray table and carried by a lift truck to the van de Graaff facilities for electron irradiation. The X-ray tube is mounted on an Economy Engineering Company elevating table which allows the X-ray tube to be moved in a vertical (z) direction. The x, y, and z coordinates were read from Starrett dial indicators with .01 mm divisions and 25 mm total travel.

The cryostat and x-y motion is supported by a plate resting on a race of 3/4" diameter steel balls on a 28" diameter circle. A bearing keeps the center of the circle true to .05 mm. A series of lever arms with a Scherr Tumico micrometer gauge permits changes in the theta angle (Bragg angle) of 1 sec. of arc to be measured.

Figure 8. Schematic diagram of X-ray apparatus: a) table which supports entire structure; b) elevating table to raise the X-ray tube and detector with respect to the crystal (i.e. adjusts z position); c) Hamner Na I(Tl) detector and preamplifier; d) dovetail to provide rotation of the detector; e) ball bearing race for the theta rotation; f) bearing to keep the center of rotation constant; g) ball bushings and rods to move cryostat in x and y directions; h) holders for X-ray apertures and absorbers (4 in view); i) cryostat. The X-ray tube, j, is positioned by the base, k, which provides linear motion in the horizontal plane, and rotation around a vertical axis.

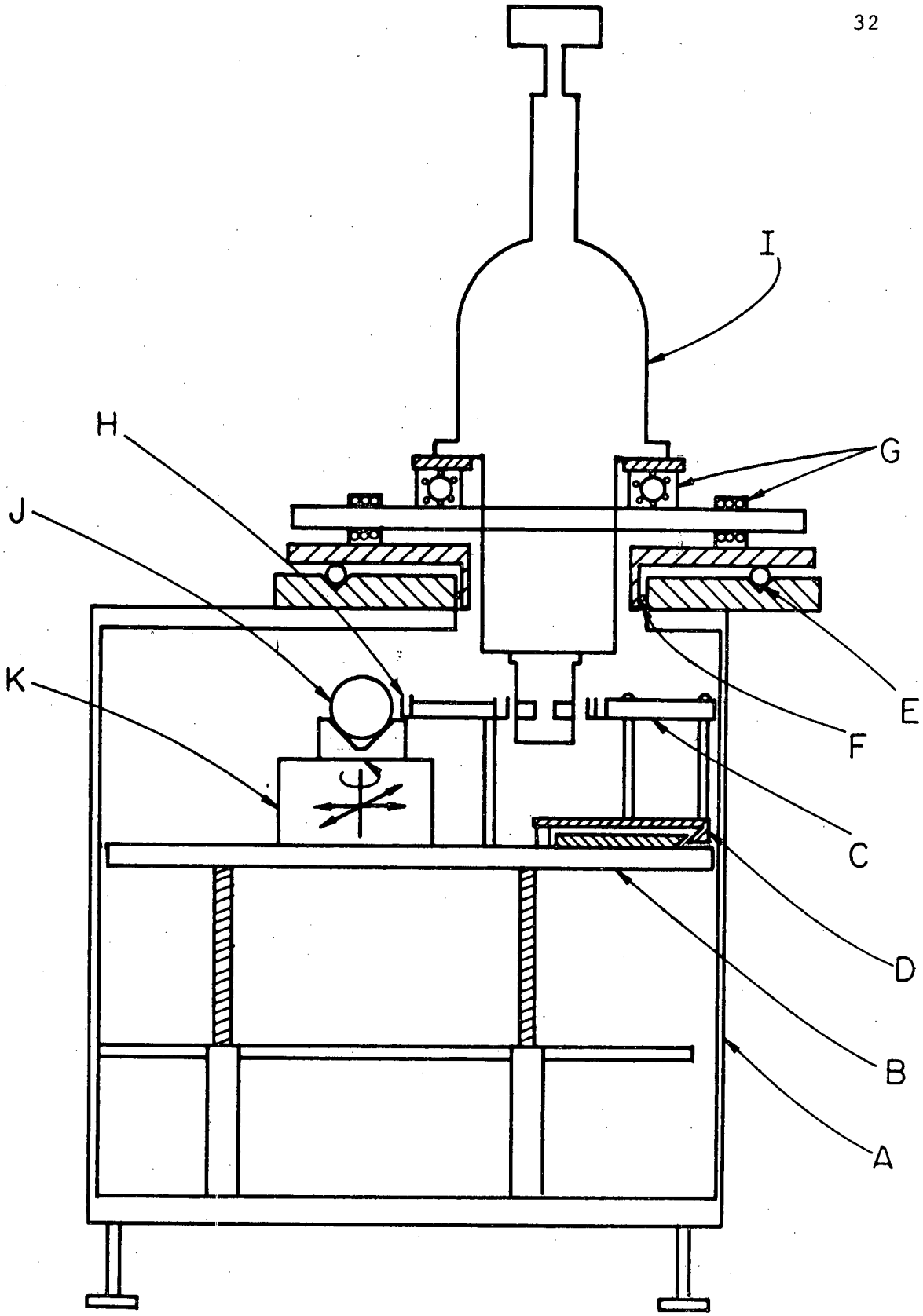
I
H
G
J
K
E
F
C
D
B
A

The arrangement of the X-ray tube, sample, and detector is shown in Figure 9. No monochromator was used in the system. This was a disadvantage because rocking curves could not be taken, and thus absolute integrated intensity measurements were unavailable. However, because the crystals were free to move in the mount, rotation of the cryostat was not necessarily the same as the rotation of the sample. In addition, the beam was found to be non-uniform as a function of position if a monochromator was used. Therefore, if the crystal moves slightly, the intensity of X-rays incident upon it varies, and since the absorption at every point is different, a slight change in position would cause a large change in the transmitted intensity. Since we were only interested in the change of X-ray intensity, an absolute integrated intensity measurement was not needed. Hirsch[35] has shown that if the incident intensity is uniform over the angular range of the dispersion surface ($\approx$ 2 seconds of arc half width in our case), the intensity will be proportional to the total integrated intensity. Therefore, the experiment could be performed without a monochromator.

The detector was positioned manually on an arm of radius 6". There were 3 apertures in the system. At the X-ray tube was a 3 mm diameter target aperture. The sample and detector apertures were replaceable and various diameter holes were used for alignment purposes. During the measurements, a 2.0 mm diameter sample aperture was used which determined the diameter of the X-ray spot at the crystal, and a 6.00 mm diameter detector aperture was used.

The X-ray tube (General Electric type CA-8) had a molybdenum target with a constant potential GE XRD 6 power supply. The detector

Figure 9. Geometry of X-ray system.

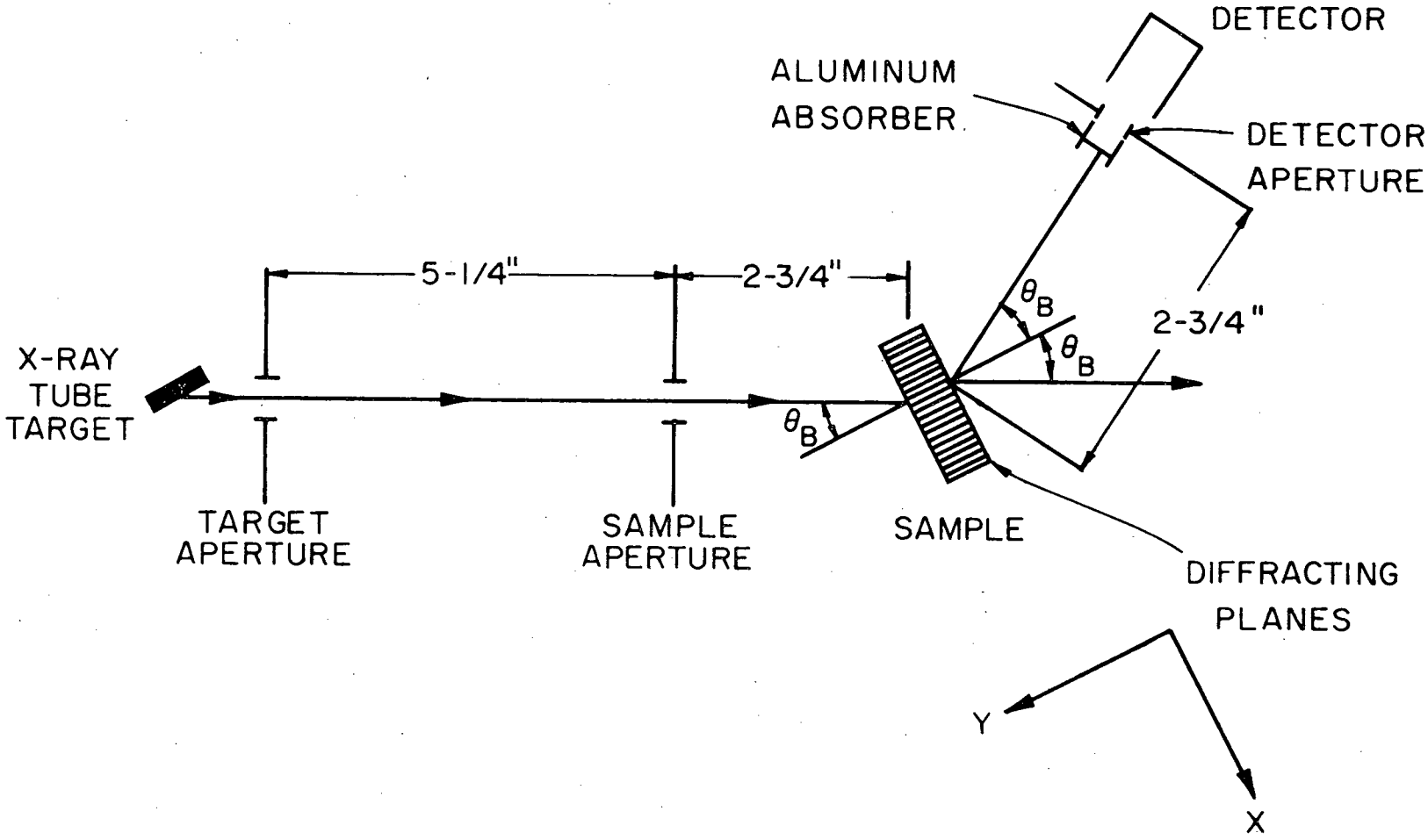
DETECTOR
ALUMINUM
ABSORBER
DETECTOR
APERTURE
5-1/4"
2-3/4"
θ_B
θ_B
2-3/4"
X-RAY
TUBE
TARGET
θ_B
TARGET
APERTURE
SAMPLE
APERTURE
SAMPLE
DIFFRACTING
PLANES
Y
X

was a Na I (Tl) Hamner detector. A Hamner NA-12 double-delay line amplifier and NC-11 pulse height analyzer were used. The count rate was printed out on a modified Beckman 1453 printer. It was found that the number of X-rays counted by the detector system was dependent on the ambient temperature of the amplifier and pulse height analyzer. Therefore, it was necessary to place the amplifier, analyzer, and detector power supply into an insulated cabinet, controlled to $\pm$ 0.1°C by a Yellow Springs Instrument #72 proportional temperature controller. Tests were then made of the counting rate and it was determined that after a three hour warm-up time of the X-ray tube, the drift in anomalous X-ray intensity was less than .03% per hour.

During the experiment, the X-ray voltage and current used were 45 kV and 28 mA respectively as measured at the XRD-6 power supply for all planes except the first order (111) planes where the voltage was 40 kV. The pulse height analyzer discriminated against any $\lambda/2$ radiation, and a .006" aluminum filter was placed in front of the detector preventing the counting of low energy X-rays.

D. Procedure for Measurement

In making the alignment adjustments, each alteration is checked by observing the resulting detected count rate. Usually the adjustment is made until a maximum count rate is achieved.

The X-ray tube and the sample and detector apertures were adjusted so that the X-ray beam passed through the center of the theta rotation, and through the zero-degree division of the detector circle. Each time the cryostat was placed on the X-ray table, the y motion

(shown in Figure 9) was adjusted so that the crystal was at the center of the theta and detector rotation. This was done by using small .35 mm sample and detector apertures. The x motion was adjusted so that the edge of the crystal partially eclipsed the X-ray beam. The y motion was then adjusted so that the crystal could be rotated about the θ axis without totally eclipsing the beam. The center of the crystal was then within $\pm$ .2 mm of the center of rotation. The following method was used to measure the anomalous transmitted X-ray intensity at a given location on the crystal. The x and z coordinates were set so that the X-ray beam was nominally (within 0.2 mm) at the location to be measured. The crystal was set near the Bragg angle, θ_B, for the Mo Kα reflection to be measured, and the detector set at $2\theta_B$ to detect the beam emerging in the diffracted direction. ϕ was then adjusted until the normal to the diffracting planes was in the plane determined by the X-ray beam and the center line of the detector (i.e. one arranges matters so that the reflecting planes are vertical). This was done with a small detector aperture to within $\pm$ 0.2°, which resulted in a negligible error in the final transmitted intensity measurements.

The crystal was then accurately mapped in order to be able to reproduce the location at which the X-ray beam struck the crystal. The detector was set to zero degrees and .35 mm sample and detector apertures were used. The crystal was then moved so that $\frac{1}{2}$ the X-ray beam was eclipsed by the crystal with the X-ray beam grazing one edge of the crystal. This was done at several positions where the crystal mount was cut out. The position of the crystal could be determined in this manner

to $\pm$ .03 mm. This error was the largest source of error in the experiment. The crystal was remapped before each measurement. The accuracy of the crystal location was determined by the ability to locate the detector at exactly zero degrees and also by the unevenness of the crystal edges. Thus the position on the crystal to be measured was known only to $\pm$ .03 mm.

The Mo Kα Bragg angle was then carefully determined. A plot of intensity vs angle is shown in Figure 10. The detector was set at $2\theta_B$ to detect the diffracted beam. The half-width of the large Mo Kα peak was determined by the aperture geometry. For this experiment, a change in intensity from the peak value to 99% of the peak value was smooth and corresponded to a change of 200 seconds of arc. The location of the peak could be determined to $\pm$ 3 sec of arc, corresponding to about .01% change in intensity.

Four locations were measured in the experiment, two on the irradiated and two on the unirradiated crystal. The points were located near the center of each crystal where the intensity was nearly a constant as a function of position. Since absolute intensity measurements were not made, the intensity at the peak of the Mo Kα reflection was measured at each of the four locations, and the change in the ratio of the anomalous transmitted intensity through the irradiated crystal to that through the unirradiated crystal was determined. The detector was set at $2\theta_B$ in order to measure the intensity in the diffracted direction. In this way, since the intensities through the two crystals were nearly the same, a dead time correction to the count rate was not needed. The measurements were made within 30 minutes of each other (except for the (333) reflections) minimizing the effects of drift in the X-ray tube voltage and

Figure 10. Anomalous transmission X-ray count rate vs Bragg angle for (111) Mo Kα reflection through copper.

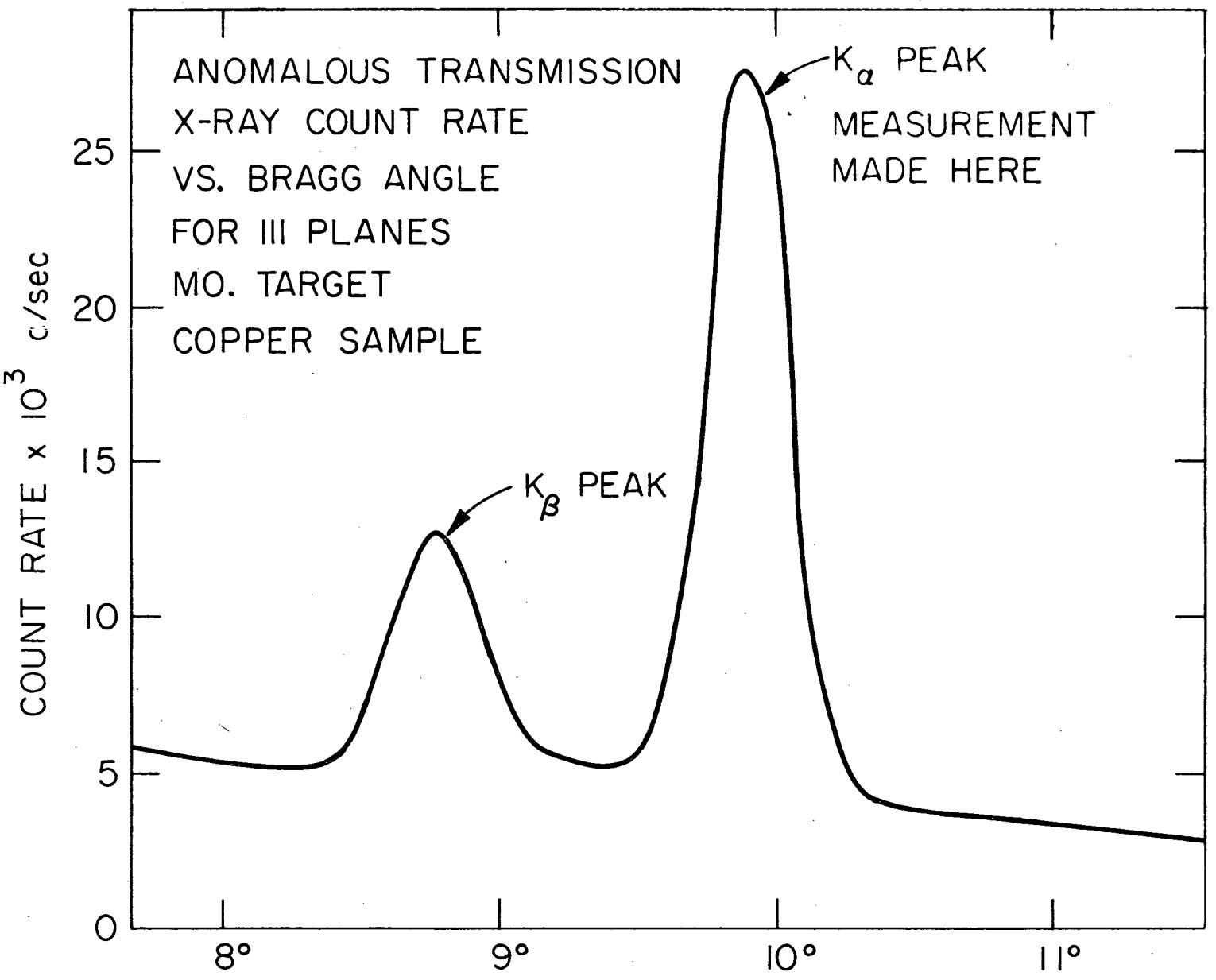
ANOMALOUS TRANSMISSION
X-RAY COUNT RATE
VS. BRAGG ANGLE
FOR III PLANES
MO. TARGET
COPPER SAMPLE
K_α PEAK
MEASUREMENT
MADE HERE
K_β PEAK
COUNT RATE x 10^3 c/sec
0
5
10
15
20
25
8°
9°
10°
11°

current. The ratio of the intensities through the two locations on the unirradiated crystal were an indication of the error in the apparatus except for the possibility of error due to the two crystals moving with respect to each other. This error is discussed in Chapter IV. In all cases, the total number of X-rays counted at each location was large enough to make the error due to random statistical fluctuations less than .03%.

The effect of long range strains on the anomalous transmission in the diffracted direction were minimized by computing the average change in intensity of the (hkl) and $(\bar{h}\bar{k}\bar{l})$ reflections. This has been justified[30,31] and will be discussed quantitatively in Chapter V. This average was obtained by measuring at both θ_B and $-\theta_B$, while the detector was moved from $2\theta_B$ to $-2\theta_B$.

Measurements were taken before irradiation, after irradiating with $.43 \times 10^{18}$ e/cm^2, and again after $.87 \times 10^{18}$ e/cm^2. The crystals were then annealed at 78°K for 48 hours and remeasured. Finally the crystals were measured after annealing at 300°K for 48 hours. All measurements were made at liquid helium temperature. The first three orders of the (111) planes and the first order of the (220) planes were measured although the (220) and (333) preirradiation measurements were not taken. In these two cases, the damage production is assumed to be proportional to flux (which is true for the (111) and (222) reflections). To check the entire procedure, the measurements were made twice after irradiation of $.43 \times 10^{18}$ e/cm^2, and the results agreed within experimental error.

E. Irradiation Procedure

The upper crystal was irradiated with 3.0 $\pm$ .1 MeV electrons, from the van de Graaff accelerator at the Materials Research Lab of the University of Illinois. After passing through a 90° bending magnet, the beam scattered from a .0005" aluminum foil 45 inches from the crystal. The foil separated the van de Graaff from the cryostat vacuum system and prevented contamination of the low temperature parts. A water cooled $\frac{1}{2}$" diameter aperture was placed 6" from the foil. The final and essentially only defining of the electron beam was done by a $\frac{1}{4}$" thick brass aperture, 1.68 cm^2 in area $1\frac{1}{2}$" from the sample. This aperture was attached to the outer rotatable cylindrical can of the cryostat (Figure 6).

The entire system was aligned by a phosphore coated screen placed behind the exit window with no sample in the mount. The vertical alignment of the aperture was also checked with the X-ray beam. The horizontal alignment was made by rotating the outer can (and hence the aperture) with respect to the sample. The beam current striking the posts on either side of the sample was collected. This current was a minimum when the aperture was aligned with the crystal.

The entire cryostat was electrically insulated from ground and acted as a Faraday cage. All electrons passing through the defining aperture passed through a current integrator to ground. The current density was obtained by dividing the current by the area of the defining aperture.

Because the samples could not be rigidly attached, the heat loss to the mount by heat conduction was very small, and the sample was

cooled primarily by means of the helium exchange gas. The dominant process was gas convection which depends on the gas pressure. Because of the softness of the crystal, it was impossible to measure the sample temperature directly by putting a thermometer on the crystal. In a test run a calibrated carbon resistance thermometer was attached to an identical dummy copper sample. The temperature of this sample was calibrated against both an identical carbon thermometer located on the mounting block, and the helium boil off rate for a variety of beam currents and exchange gas pressures. It was determined that with 1 atm. of gas pressure and .35 $\mu A/cm^2$ beam current, the sample temperature was less than 22°K, and the boil off rate was about 2 liters of liquid helium per hour. The sample temperature was, therefore, kept below 22°K during irradiation.

The total irradiation time was 120 hours, with a total flux of $.87 \times 10^{18}$ e/cm^2. After total fluxes of .21 and $.64 \times 10^{18}$ e/cm^2 the entire cryostat was rotated 180° such that the electron beam struck the opposite face of the crystal. This was done to reduce the strains in the crystals due to defect concentration gradients. Since the electrons lost about 1.0 MeV in traversing the crystal, the total displacement cross-section (including secondary displacements) went from about 120 barns at the entering face to about 90 barns at the exit face for a displacement threshold energy of 22 eV.[36] Thus, the concentration of defects is less at the back surface of the crystal than near the front surface. This is partially compensated for by the Yang correction[8] because the path length (and hence the damage production) is larger near the back face due to multiple scattering. Because of the neutron hardening, the

strain due to the defect concentration gradient will be elastic for reasonably small concentrations. Thus, by irradiating with half the flux incident on one surface and half the flux incident on the opposite surface, the concentration gradients were made smaller. Calculations show that for a flux of $.87 \times 10^{18}$ e/cm^2 the concentration was a maximum at the center of the crystal and the defect concentration gradient from the center to either surface was about 2×10^{-6}. This was not large enough to affect the anomalous transmitted intensity.

IV. EXPERIMENTAL RESULTS

The change in the intensity of anomalously transmitted X-rays was obtained by taking the ratio of the count rate at one location (referred to as location 3) on the irradiated crystal to the count rate at one location on the unirradiated crystal (location 2). The percentage change of the ratio is shown in Figures 11-14. The left side of these graphs shows the change caused by the irradiation and is plotted as a function of integrated electron flux. The right side shows the recovery as a function of annealing temperature. The values plotted are the average of the change in the (hkl) and $(\bar{h}\bar{k}\bar{l})$ reflections. The results are also shown in Table 1.

If R_{hkl} is the count rate for the (hkl) reflection and

$$\bar{R}_{hkl} = \frac{R_{hkl} + R_{\bar{h}\bar{k}\bar{l}}}{2} \tag{31}$$

is the average count rate, then a measurement of the long range strains present (strains where the lattice parameter varies slowly with respect to an extinction distance) can be given by

$$\Delta_{hkl} = \frac{R_{hkl} - R_{\bar{h}\bar{k}\bar{l}}}{\bar{R}_{hkl}} \quad . \tag{32}$$

Figure 15 shows Δ_{222} during the experiment. The significance of Δ_{hkl} will be discussed in section V. It will be shown that the change in Δ_{hkl} is so large at location 4 (the other measured location on the irradiated crystal) that the change in $\bar{R}_{hkl}$ due to long range strains was large. Therefore, some of the change in intensity at location 4 was due to slowly varying strain fields rather than point defects. It will

Figure 11. Decrease in anomalously transmitted intensity for the (111) reflection. The left side of the figure shows the intensity decrease vs electron flux. The right side shows the intensity decrease vs annealing temperature.

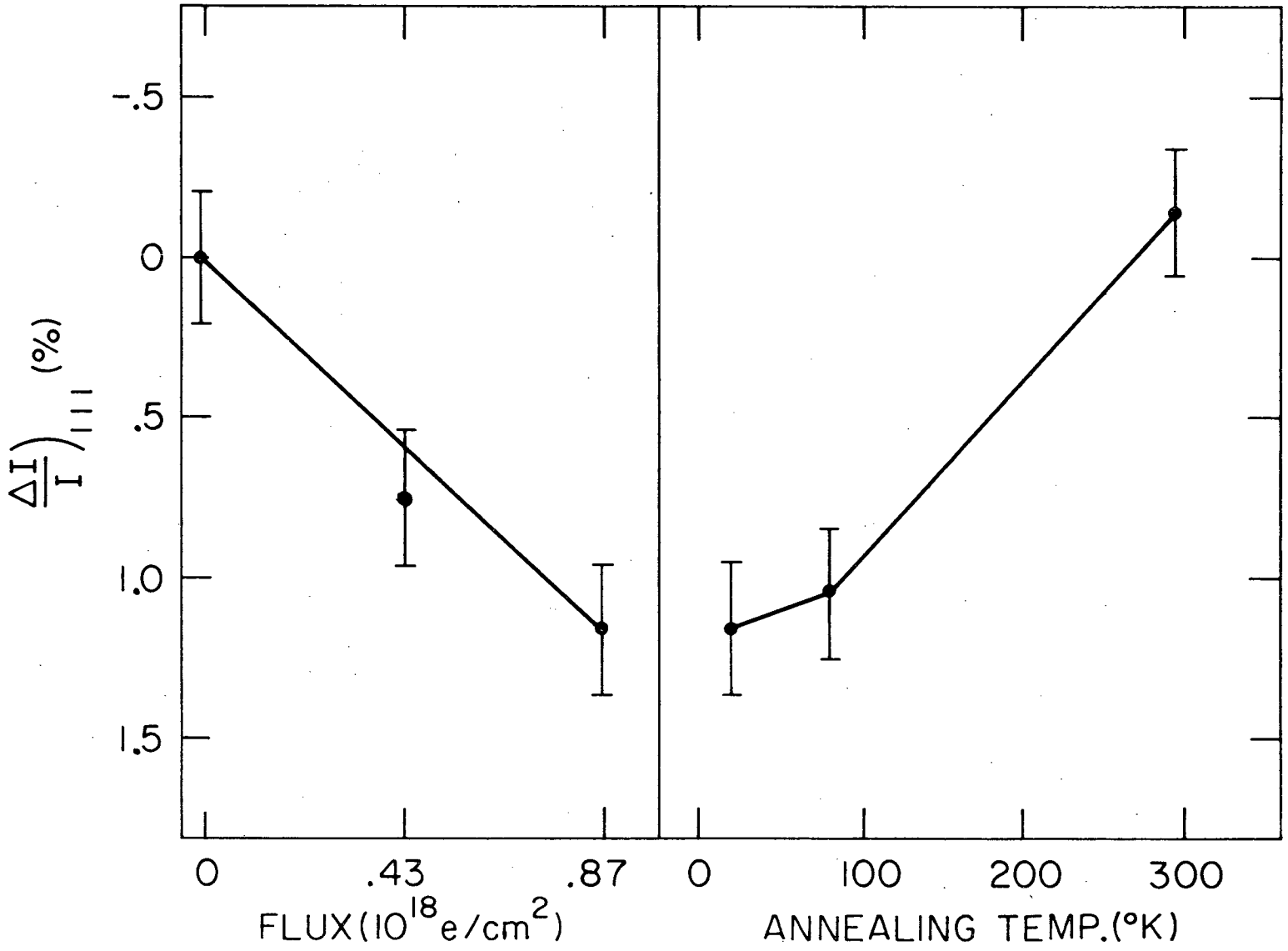
-.5
0
.5
1.0
1.5
$\frac{\Delta I}{I}\Big)_{111}$ (%)
0
.43
.87
FLUX(10^{18}e/cm^2)
0
100
200
300
ANNEALING TEMP.(°K)

Figure 12. Decrease in anomalously transmitted intensity for the (222) reflection. The left side of the figure shows the intensity decrease vs electron flux. The right side shows the intensity decrease vs annealing temperature.

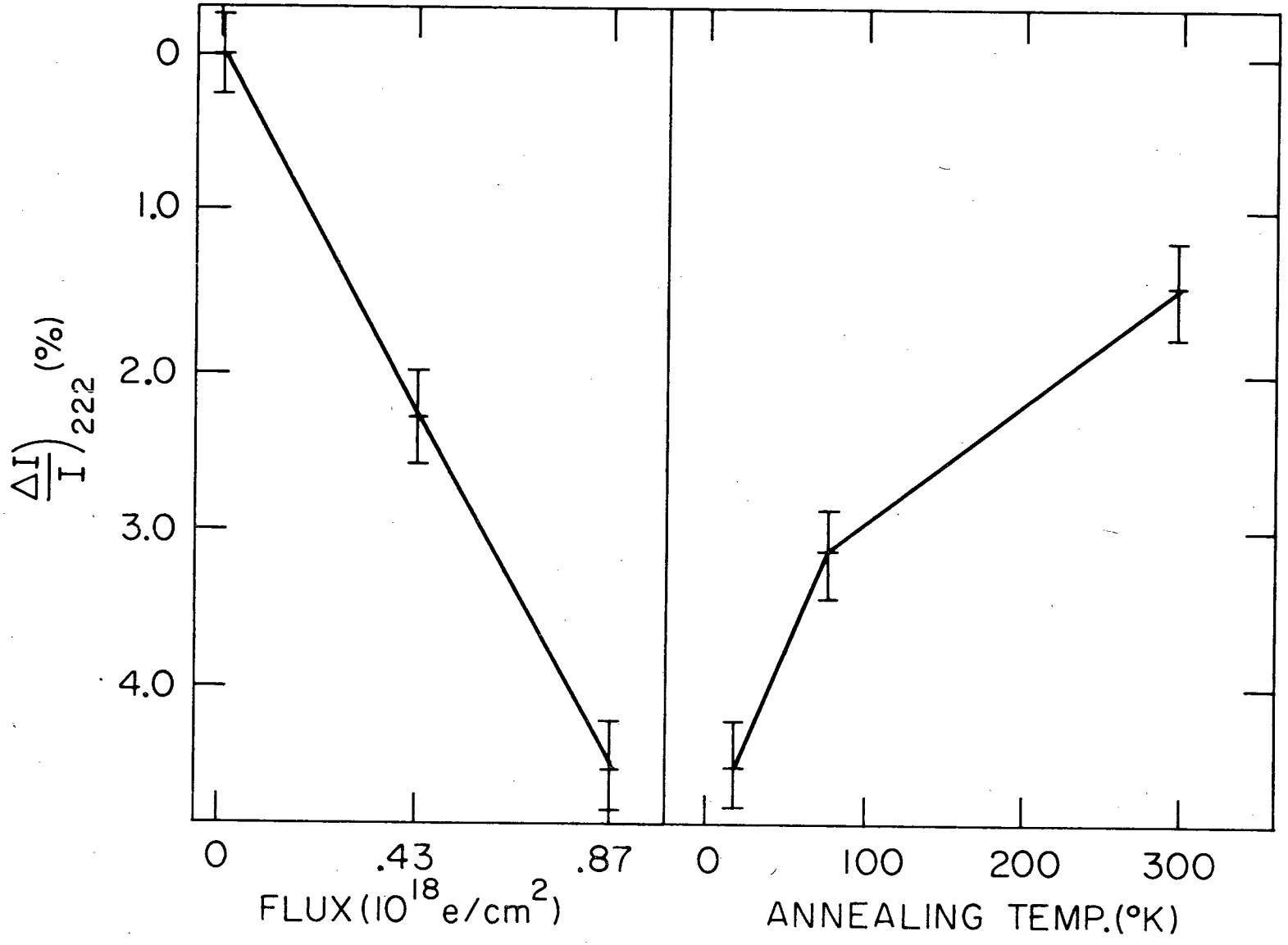
0
1.0
2.0
3.0
4.0
$\frac{\Delta I}{I}_{222}$ (%)
0
.43
.87
FLUX (10^{18} e/cm^2)
0
100
200
300
ANNEALING TEMP.(°K)

Figure 13. Decrease in anomalously transmitted intensity for the (333) reflection. The left side of the figure shows the intensity decrease vs electron flux. The right side shows the intensity decrease vs annealing temperature.

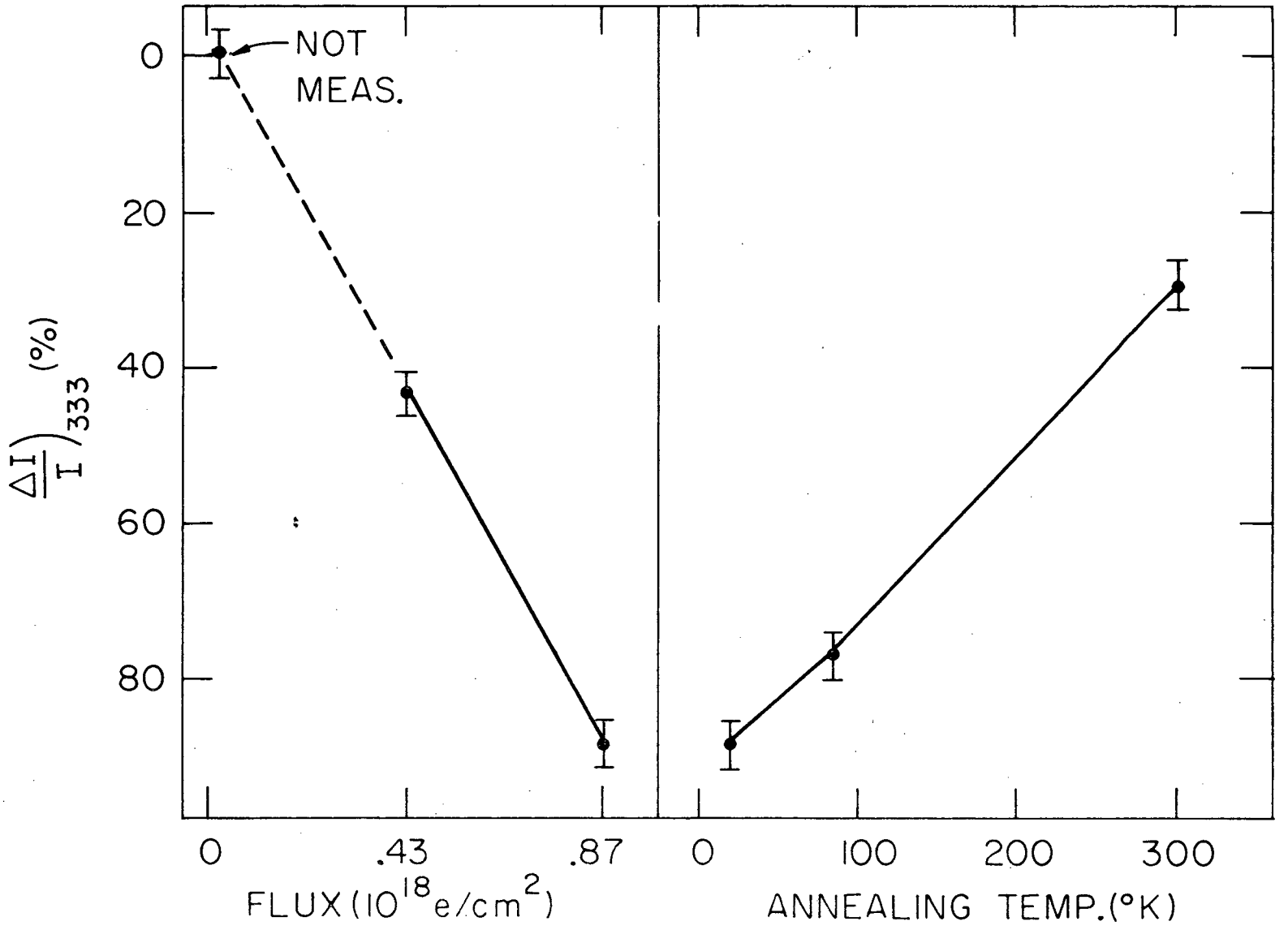
NOT
MEAS.
0
20
40
60
80
$\frac{\Delta I}{I}\Big)_{333}$ (%)
0
.43
.87
FLUX (10^{18} e/cm^2)
0
100
200
300
ANNEALING TEMP.(°K)

Figure 14. Decrease in anomalously transmitted intensity for the (220) reflection. The left side of the figure shows the intensity decrease vs electron flux. The right side shows the intensity decrease vs annealing temperature.

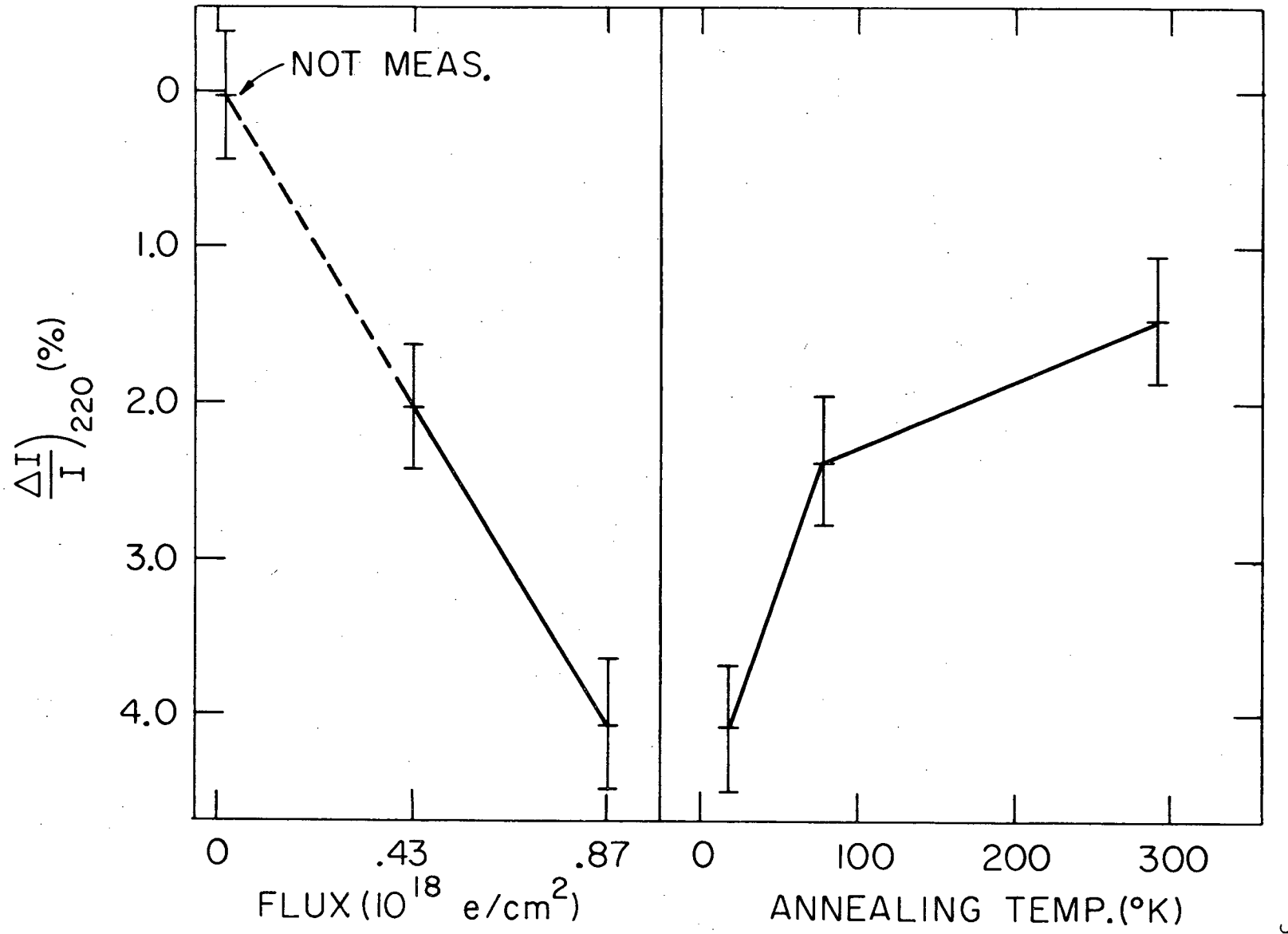
NOT MEAS.
0
1.0
2.0
3.0
4.0
$\frac{\Delta I}{I})_{220}$ (%)
0
.43
.87
FLUX (10^{18} e/cm^2)
0
100
200
300
ANNEALING TEMP.(°K)

Figure 15. The percentage difference in intensity, Δ_{222} (Eq. (32)), between the (222) and $(\bar{2}\bar{2}\bar{2})$ reflection. The left side of the graph shows Δ_{222} as a function of electron flux, and the right side shows Δ_{222} as a function of annealing temperature.

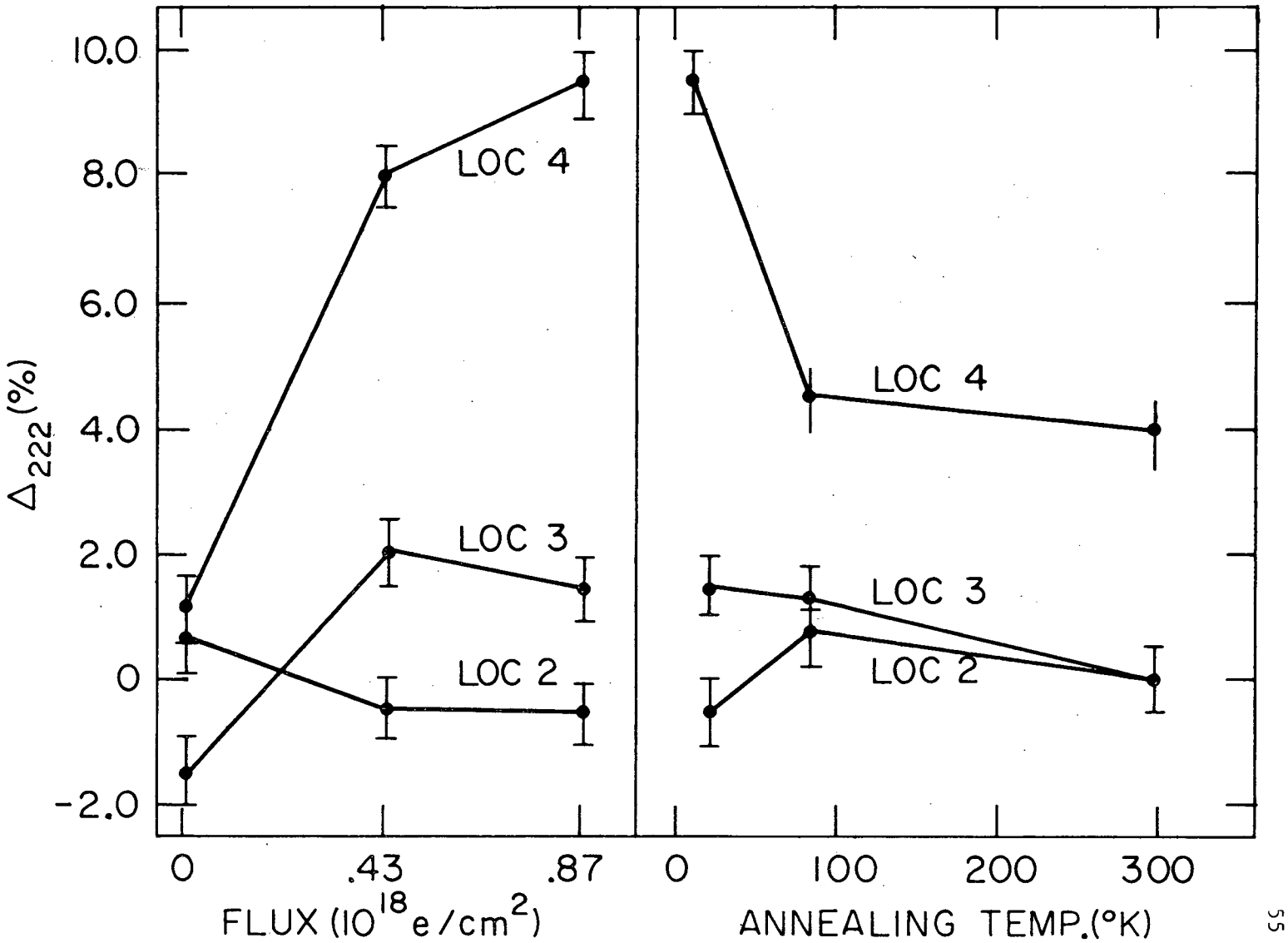
10.0
8.0
6.0
4.0
2.0
0
-2.0
Δ_{222}(%)
LOC 4
LOC 3
LOC 2
0
.43
.87
FLUX (10^{18} e/cm^2)
LOC 4
LOC 3
LOC 2
0
100
200
300
ANNEALING TEMP.(°K)

Table 1

Experimental Decrease in Intensity With Respect to Unirradiated Crystal

Reflecting Planes	After Irradiation	After Anneal at 80°K	After Anneal at 300°K	% Recovery After Anneal at 300°K
111	1.15 ± .4%	1.05 ± .4%	-.13 ± .4%	112%
222	4.52 ± .6%	3.15 ± .6%	1.44 ± .6%	68%
333	8.90 ± .8%	7.68 ± .8%	3.00 ± .8%	66%
220	4.06 ± .8%	2.41 ± .8%	1.35 ± .8%	67%

be shown that the results of strain at location 3 produce negligible change in $\bar{R}_{hkl}$ and, therefore, do not effect the change in intensity due to point defects. Therefore, only the results of the change at location 3 were used in Figures 11-14. There are two possible reasons for the large strain present at location 4. One is the possibility of the electron irradiation being non-uniform in the region of this location. Another possible reason is that location 4 was in a region of larger surface curvature as discussed in section III. The larger surface curvature causes the effect of a small strain on the anomalous transmission to be larger at location 4 than the effect of an equal amount of strain at location 3 which is in a region of smaller curvature.

There were three types of error in the experiment. The first type was the change in intensity due to strains in the irradiated crystal which might have changed during the irradiation. This was a small change at location 3, and will be discussed in section V. A second type of error arises from a statistical fluctuation of X-ray tube voltage, changes in room temperature with time, counting statistics, errors in the determination of angle or position, etc. Errors of this type would be the same in the unirradiated crystal as in the irradiated crystal. Thus, by measuring the changes in the ratio of the two locations on the unirradiated crystal throughout the experiment, we obtained the error (standard deviation) present due to all such factors. The third type of error is due to motion of the two crystals with respect to each other. The location of the crystals was known to $\pm$.03 mm and the change in intensity as a function of position near the locations was carefully measured.

Thus the error due to the uncertainty in position could be determined. The total resulting error is shown in Table 1.

It has been suggested that local modes of oscillation of the interstitial and surrounding lattice exist. Also, since the Debye-Waller factor for a displaced atom is not the same as for a lattice atom, one might expect that the temperature dependence of the irradiated and unirradiated samples might be different. Therefore, the ratio of the anomalous X-ray intensity through the irradiated crystal to the intensity through the unirradiated crystal was taken at 4.2° and $11.2^{\circ}K$ to see if the ratio changed. This was after a total flux of $.87 \times 10^{18}$ e/cm^2. No noticeable change occurred. Thus the assumption that $\epsilon_h = \epsilon_{oh} e^{-M}$ for both the irradiated and unirradiated crystal appears to be justified.

V. CALCULATIONS AND DISCUSSION

Eight possible equilibrium configurations of the interstitial are shown in Figure 16, where the notation is that of Seeger et al.[10] and Johnson.[14] The energies and displacements associated with these configurations have been treated theoretically using a wide variety of models. Johnson[37] points out that the calculations are essentially computer "experiments," and a comparison of the models involves a discussion of accuracy. For example, the results depend critically on the computational cell size. Nevertheless, the displacements associated with the various configurations are significantly different and should be compared with experiment. In region 1 the displaced atoms are close to the center of the interstitial configuration and the atoms cannot be adequately described in terms of linear elastic theory. The displacements are large and must be treated as discrete particles. Several authors[9-14] have published calculations. The resulting displacements can be put directly into the sum of Eq. (21). The results of some of the most detailed calculations are shown in Table 2. In each case it is assumed that the interstitials are isotropically distributed over all possible orientations (e.g. the (100) split interstitial can lie along 3 different (100) directions).

The number of atoms included in region 1 and the distance of the farthest atom in region 1 from the interstitial (r_{min}) are also shown in Table 2.

The displacement of atoms in the elastic continuum (region 2) must also be considered in the calculations. In continuum theory,

Figure 16. Eight basic interstitial configurations: H_O is the (100) split configuration; O is the body-centered configuration which has octahedral symmetry; H_T is the (111) split configuration; T is the configuration with tetrahedral symmetry; H_C is the (110) split, or split crowdion configuration; C is the crowdion configuration; OC is the configuration in which the interstitial lies on the line between O and C configuration, nearer to O; and OT is that in which the interstitial lies on the line between O and T, nearer to O. The relaxation of neighboring atoms to the interstitials is not shown.

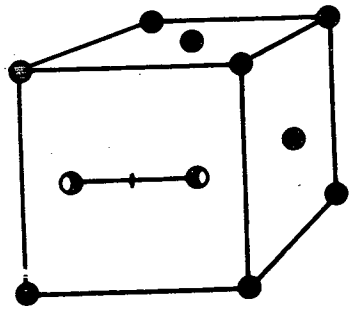

H_O

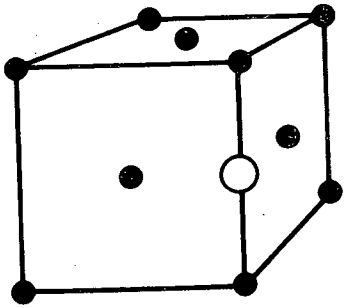

O

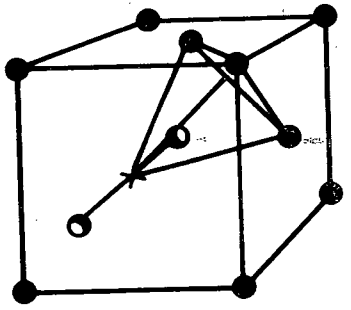

H_T

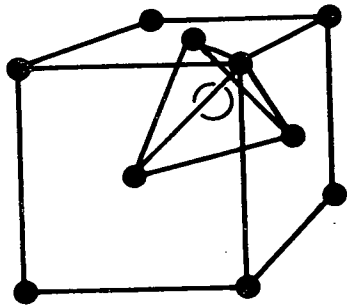

T

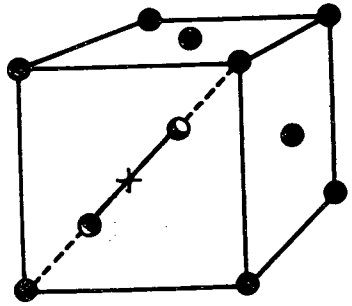

H_C

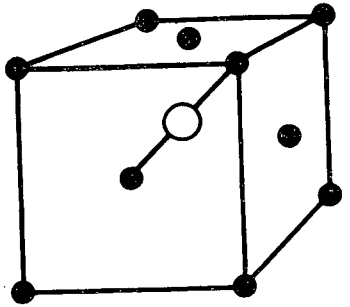

C

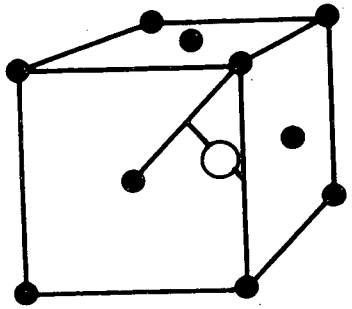

OC

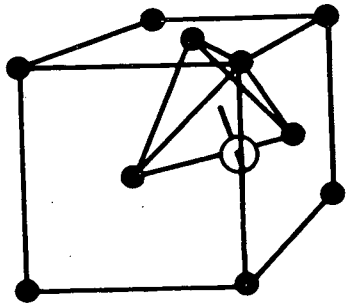

OT

Table 2
The Effect of Displaced Atoms in Region 1
on the Anomalous Transmission of X-rays

Type of Defect	Displacements used	No. Atoms in Region 1	r_{min} a	$\sum_j (1-\cos(\underset{\sim}{h}\cdot\underset{\sim}{r}_{oj}))$ Reflecting Planes			
				111	222	333	220
O	Johnson*[43]	267	2.5	3.11	7.85	17.67	5.23
	Doyama[11]	117	1.8	3.82	6.69	15.07	4.36
	Tewordt[12]	88	1.8	4.67	9.43	19.28	6.41
H_o	Johnson*[43]	250	2.4	3.89	8.65	10.19	5.97
	Doyama[11]	56	1.4	3.83	8.64	10.12	6.01
	Benneman[a13]	74	1.6	4.16	9.07	10.70	6.21
H_T	Doyama*[11]	53	1.4	3.48	8.03	13.72	5.78
	Benneman[a13]	34	1.2	3.77	7.77	10.94	5.52
H_C	Johnson[14]	16	1.4	3.54	4.63	5.42	4.57
	Doyama*[11]	56	1.2	3.56	5.50	8.08	6.53
T	Johnson[14]	29	1.2	3.97	9.71	12.75	6.14
	Doyama*[11]	71	1.6	3.67	9.54	12.85	5.88
Vacancy	Doyama*[11]	54		.131	.519	1.15	.412

*Values used in Table 3.

[a]Using displacements associated with the Born-Mayer potential.

assuming an isotropic medium, the displacement field of an "isotropic" point defect is

$$\underset{\sim}{r}_{oj}(\underset{\sim}{r}) = A \frac{\underset{\sim}{r}}{r^3} \quad . \tag{33}$$

Where $\underset{\sim}{r}_{oj}(\underset{\sim}{r})$ is the displacement of atom j which is located at a distance $\underset{\sim}{r}$ from the defect. A is related to the volume change ΔV by

$$\Delta V = 4\pi A \frac{3(1-\nu)}{(1+\nu)} \quad , \tag{34}$$

where ν is Poisson's ratio.

In region 2, the displacement $\underset{\sim}{r}_{oj}$ is small and the sum in Eq. (21) becomes

$$\sum_j (1-\cos(\underset{\sim}{h}\cdot\underset{\sim}{r}_{oj})) \cong \sum_j \tfrac{1}{2}(\underset{\sim}{h}\cdot\underset{\sim}{r}_{oj})^2 \quad . \tag{35}$$

If we convert the sum to an integral over region 2, which includes all atoms farther from the interstitial than a minimum distance r_{min}, we get

$$\sum_j (1-\cos(\underset{\sim}{h}\cdot\underset{\sim}{r}_{oj})) \cong \frac{2\pi}{3} \frac{A^2 |\underset{\sim}{h}|^2}{r_{min}} \frac{4}{a^3} \tag{36}$$

where a is the lattice constant, and there are $4/a^3$ atoms per unit volume. If we assume $\nu = 1/3$ for copper, and $V \cong \frac{a^3}{2}$ 38/ for a single interstitial, we get

$$A \cong .03a^3 \tag{37}$$

and

$$\sum_j (1-\cos(\underset{\sim}{h}\cdot\underset{\sim}{r}_{oj})) \cong \frac{0.3a}{r_{min}} (h^2 + k^2 + l^2) \quad . \tag{38}$$

Thus the contribution to Eq. (21) from all atoms farther from the interstitial than r_{min} is

$$\left(\frac{\Delta I}{I}\right)_{\text{region 2}} = \frac{\mu_o t}{\cos \theta_B} \epsilon_h C_i \frac{0.3a}{r_{min}} (h^2 + k^2 + l^2) \ . \qquad (39)$$

The values of r_{min} are shown in Table 2. In each case, region 2 is taken to be the atoms not included in the calculation of region 1. Thus r_{min} is given by the distance from the interstitial of the farthest atom included in region 1 for each calculation.

Several approximations have been made in deriving this equation. The copper lattice is not isotropic. Thus the displacement field should be represented by a more complicated expression.[39] Also the field around several of the configurations shows other than spherical symmetry (e.g. the (100) split interstitial). There are also corrections to the displacement field of order $1/r^4$. The volume change ΔV is not accurately known and may be different for different interstitial configurations.

The choice of this one term as the only contribution to the elastic displacement field is discussed in detail by Johnson and Brown[9] who point out that the atomic configurations near defects are insensitive to other solutions of the isotropic elastic equation and it has been shown[40] that anisotropic solutions do not play a large role. Since region 2 represents only a small part of the total intensity change, the isotropic elastic solution is probably a valid approximation.

Several constants in Eq. (21) have been determined. μ_o has been measured experimentally for similar copper crystals for MoKα X-rays with the result[41]

$$\mu_o = 438 \text{ cm}^{-1} .$$

It has been shown[16] that

$$\frac{(1 - \epsilon_{oh})}{(1 - \epsilon_{oh'})} = \frac{d^2_{h'k'l'}}{d^2_{hkl}} . \tag{40}$$

Experimental values of ϵ_{oh} for the (111), (222), and (220) reflections have been determined[41] and fit Eq. (40) very well. Equation (40) has been used to evaluate ϵ_{oh} for the (333) reflection.

The Debye-Waller factor, M, is given by

$$M = \frac{6h^2T}{mk\theta_d^2} \left(\Phi(X) + \frac{X}{4}\right) \frac{\sin \theta_B}{\lambda} \tag{41}$$

where h is Planck's constant, T is the temperature of the crystal, m is the mass of the copper atom, k is Boltzmann's constant. θ_d is the Debye temperature which has been determined experimentally[41] to be equal to 300°K for X-ray measurements in copper. $\Phi(X)$ is the Debye function, where $X = \frac{\theta_d}{T}$. For low temperatures, $(\frac{\theta_d}{T} \gg 1)$, $\Phi(X) \ll \frac{X}{4}$, and the equation is essentially independent of temperature.

The X-ray wavelength $\lambda = .71$ Å for MoKα X-rays. Thus we find

$$M_{hkl} \cong 2.88 \times 10^{-3}(h^2 + k^2 + l^2) . \tag{42}$$

The concentration of interstitials C_i is difficult to determine. The displacement cross sections have been calculated for copper by O. S. Oen[36] using relativistic scattering theory. The calculation follows closely that of Seitz and Koehler.[42] Included in the calculations is the effect of the secondary displacements being produced.

Using a displacement threshold energy of 22 eV,[8] and correcting the production cross section by using the Yang correction,[8] we obtain a total average cross section of $\sigma_d = 120$ barns, including secondary displacements. This result is not to be taken too seriously. The threshold energy is not well known, and is different for different recoil directions. The energy loss of the primary displaced atoms is not well known and, therefore, the number of secondary displacements is not accurately known. Thus the cross section for actual damage production might be in error by a factor of 2. However, assuming a flux of $.87 \times 10^{18}$ e/cm^2 we obtain an initial concentration of $C_i = 1 \times 10^{-4}$.

The effect of the vacancy on the anomalous transmission is much smaller than that of the interstitial. In the previous calculation it was assumed that the effect of an interstitial atom was the same as that of a displaced atom. Thus the "vacancy" was already included in the calculation. There is, however, a change in intensity due to atoms collapsing around the vacancy. Using the displacements of Doyama,[11] calculations can be made of the effect of the vacancies on the anomalous transmission.

No calculations have been made using the fact that the displacements around a Frenkel pair are different from the displacements around isolated interstitials and vacancies. Since the displacements around a vacancy are small, and since the closest interstitial-vacancy pairs are unstable,[14] and also since the closest stable pairs (stage I_A) anneal at a temperature below 20°K (hence during the electron irradiation), the displacements around the interstitials present after irradiation are not altered very much by the presence of the vacancy.

The results of the calculations are shown in Table 3. The result includes the change due to the displaced atoms in region 1 (from the values of Table 2), the displaced atoms in region 2 (Eq. (39)), and the displaced atoms around the vacancies. These numbers are based on a defect concentration of 1×10^{-4}.

Since the concentration of defects is not accurately known, it is the ratios of the changes for various orders of reflection that are more meaningful numbers to compare with experiment. These are also shown in Table 3.

Although the results of Table 3 depend on the concentration of defects introduced, it is clear that the results are not inconsistent with experiment. The ratios of the intensity changes indicate that the (100) split interstitial models do not agree with the results of the experiment. This is true in all of the calculations and is especially apparent in the ratio of the intensity change of the third order (111) reflection to the change in the second order (111) reflection, which is independent of defect concentration. The body centered interstitial model does fit the data within experimental error, and the calculations of Doyama and Cotterill[11] indicate that the (111) split interstitial model also fits the data. More samples will have to be measured in order to decrease the experimental error and thereby enabling the configuration of the interstitial to be determined more precisely.

The change in the anomalous transmission due to strains has been discussed by Penning and Polder,[31] and by Okkerse and Penning.[30] They extend the dynamical theory of X-ray diffraction to include the case where the lattice parameter varies slowly with respect to the

Table 3

Intensity change, $\left(\frac{\Delta I}{I}\right)_{hkl}$, in %, due to interstitial-vacancy pairs

hkl	ϵ_o	e^{-M}	Calculated (based on $C_i=C_V=10^{-4}$) type of interstitial O	H_o	H_T	H_C	T	Experiment
111	.998	.991	1.38	1.69	1.61	1.68	1.66	1.15 ± .4
222	.993	.966	3.80	4.13	4.26	3.41	4.75	4.52 ± .6
333	.985	.926	8.86	5.87	8.16	6.21	7.57	8.90 ± .8
220	.995	.977	2.53	2.83	3.00	3.39	2.97	4.06 ± .8

Ratios of intensity change $\frac{\left(\frac{\Delta I}{I}\right)_{h'k'l'}}{\left(\frac{\Delta I}{I}\right)_{hkl}}$

$\frac{h'k'l'}{hkl}$	Calculated Type of Interstitial O	H_o	H_T	H_C	T	Experiment
$\frac{222}{111}$	2.75	2.44	2.65	2.03	2.86	3.93 ± 1.8
$\frac{333}{222}$	2.33	1.42	1.92	1.82	1.59	1.97 ± .4
$\frac{222}{220}$	1.50	1.45	1.42	1.01	1.60	1.11 ± .4

extinction distance. For the case where the count rate is proportional to the integrated intensity, they obtain the results:

$$\ln \frac{T}{T_o} = -\frac{1}{6} P^2 \left(C + \frac{3}{2}\right) \tag{43}$$

$$\ln \frac{R}{T} = 2 \ln \left(\sqrt{1 + P^2} - P\right) - \left(2\sqrt{1 + P^2} - P\right) C^{-1} \tag{44}$$

where $C = \frac{\mu_o t}{\cos \theta_B} \epsilon_h \cong 40 \gg 1$ for this experiment, R and T are the count rates in the diffracted and incident directions after straining, and T_o is the count rate in the incident direction before straining (see Fig. 1).

P is a parameter depending on the kind of deformation of the crystal. It is also proportional to the angle the diffracting planes make with the surface of the crystal. For example, if the crystal is deformed by a bending moment,

$$P = \frac{\delta}{\psi_h R} \tan \theta_B (1 + (1 + \nu) \cos^2 \theta_B) t \tag{45}$$

where δ is the small angle between the normal to the surface and the reflecting planes, R is the radius of curvature of the sample, ν is Poisson's ratio, and ψ_h is the atomic scattering factor for the reflection under consideration. For small strains, P is small and Eqs. (43) and (44) can be expanded to give

$$R \cong R_o (1 + 2P + 9P^2 + \cdots) \tag{46}$$

where R_o is the intensity in the diffracted direction before straining. If the crystal is bent by the mount or by the radiation damage, or if a temperature gradient exists in the crystal, P is an odd function of θ_B

and therefore

$$P_{\theta_B} = -P_{-\theta_B} . \tag{47}$$

Thus by taking an average of R_{hkl} and $R_{\bar{h}\bar{k}\bar{l}}$ we eliminate the effect of strain to first order in P. By taking the value of

$$\frac{R_{hkl} - R_{\bar{h}\bar{k}\bar{l}}}{R_o} \cong 4P \cong \Delta_{hkl} \tag{48}$$

we can then determine the decrease in intensity

$$\left(\frac{\Delta I}{I}\right)_{hkl} \approx 9P^2 \tag{49}$$

due to strain. The results show that a negligible change due to strain occurs for the (111), (222), and (220) reflections but as much as 0.4% change is possible for the (333) reflection. This is less than 5% of the measured change.

The results of the annealing can only be discussed qualitatively. Studies of the recovery of electrical resistivity produced by electron-irradiation of copper show that only a small fraction ($\approx$ 20%) of the resistivity increase remains after warming to 60°K. In addition, most of the electrical resistivity remaining at 60°K recovers during stage III annealing which occurs at $\approx$ 300°K.

This is not the case in the X-ray measurement. Only a small amount of recovery occurs below 80°K and, with the exception of the first order (111) reflection, about 30% of the induced intensity change still remains after warming to 300°K.

This discrepancy can be explained in terms of the clustering of defects. A cluster of interstitials forming a loop has a lower

electrical resistivity than the same number of isolated interstitials. However, the results of section 2 indicate that the X-ray intensity change caused by a dislocation loop is much greater than the same number of isolated interstitials. Based on experiments comparing the resistivity present after irradiation at 20° and subsequent anneal at 80°K, with the resistivity present after irradiation with the same flux at 80°K,[8] it has been argued that interstitial clustering occurs below 80°K. Therefore, the data of the present experiment can be explained by assuming that although all of the close Frenkel pairs recombine during Stage 1, the remaining interstitials can form clusters causing a large change in intensity. Unfortunately, neither the number of clusters nor the radius of the clusters are known. Therefore, quantitative comparison of theory and experiment cannot be made at this temperature. It is interesting to note that the recovery of the X-ray intensity change was large in the (220) reflection which is consistent with Shimomura's finding[21] that the clusters exist as dislocation loops in the (111) planes.

Scheidler and Roth[23] have made electron microscope studies of defect clusters in 3 MeV electron irradiated copper. Although most of the irradiation was done at 120°K and above, one measurement was made on a specimen irradiated at 15°K. They find upon warming up to room temperature a defect cluster concentration of 2.7×10^{-7} after a flux of 2.9×10^{19} e/cm^2. Unfortunately, the size and concentration of the clusters as a function of flux is not known for the sample irradiated at 15°K. One would expect a much different relationship to hold for the samples irradiated below Stage I where the mechanisms of clustering

are different than for samples irradiated above Stage I. For example, di-interstitials may be formed upon annealing through Stage I without the presence of impurities.[8] However, if we assume an average cluster size of 20 Å in diameter which is consistent with Scheidler and Roth's data in samples irradiated at 130°K, and if we assume that the cluster concentration is a linear function of flux for the 15°K irradiated crystals, we would expect a cluster concentration of about 1×10^{-8}.

Results of the data of Baldwin, Sherrill, and Young[6] on fast neutron irradiation of copper indicate that for a concentration $C_1 = 6 \times 10^{-8}$ of dislocation loops with an average radius equal to 20 Å, the experimental value of the effective linear absorption coefficient for the (111) reflection with MoKα X-rays is given by

$$\mu^* \cong 4\text{cm}^{-1} . \tag{50}$$

Thus, by using the results in section 2 of the change in intensity due to loops we expect for the intensity change in the (hkl) reflection

$$\frac{\Delta I}{I} \cong (4\text{cm}^{-1})\ t \left[\frac{R_o}{20\text{Å}}\right]^3 \frac{C_1}{6 \times 10^{-8}} \left[\frac{h^2 + k^2 + l^2}{3}\right]^{3/4} . \tag{51}$$

Using the values $t = .9\text{mm}$, $R_o = 10$ Å, and $C_1 = 10^{-8}$, we obtain

$$\left(\frac{\Delta I}{I}\right)_{hkl} \cong .7 \left[\frac{h^2 + k^2 + l^2}{3}\right]^{3/4} \% . \tag{52}$$

This does not agree with the results of the (111) reflection but for the other sets of planes (i.e. (222), (333), (220)), the results agree remarkably well with the data. However, there are so many assumptions made in the calculations that it is quite fortuitous that the results agree this well.

The fact that the intensity in the (111) reflection completely recovers is inconsistent with the results of the other reflecting planes, and cannot be explained at this time.

VI. SUMMARY AND CONCLUSIONS

3 MeV electron irradiation at 20°K in nearly perfect copper crystals (essentially zero dislocations/cm^2) has been investigated by anomalous transmission intensity measurements. These measurements demonstrate that anomalous transmission can be used to determine structural nature of point defects. They indicate that the interstitial present at low temperatures in copper is not the split (100) interstitial. However, additional measurements will be required in order to decide on the exact nature of the interstitial.

Moreover, since anomalous transmission is very sensitive to the clustering of defects, information is given concerning the interstitial clusters forming during the stage I_E long range migration and partially disappearing at higher temperatures.

LIST OF REFERENCES

1. J. R. Pattel and B. W. Batterman, J. Appl. Phys. 34, 2716 (1963).

2. O. N. Efimov and A. M. Elistratov, Soviet Phys.-Solid State 4, 2131 (1963).

3. S. Maruyama, J. Phys. Soc. Japan 20, 1399 (1965).

4. R. Collella and A. Merlini, Phys. Stat. Sol. 14, 81 (1966).

5. T. O. Baldwin and J. E. Thomas, J. Appl. Phys. 39, 4391 (1968).

6. T. O. Baldwin, F. A. Sherrill, and F. W. Young, Jr., J. Appl. Phys. 39, 1541 (1968).

7. B. W. Batterman, Phys. Rev. Letters 22, 703 (1969).

8. For a discussion, see J. W. Corbett, "Electron Radiation Damage in Semiconductors and Metals," Solid State Physics, Supp. 7, F. Seitz and D. Turnbull, eds., Academic Press, New York (1966).

9. R. A. Johnson and E. Brown, Phys. Rev. 127, 446 (1962).

10. A. Seeger, E. Mann, and R. J. v Jan, Phys. Chem. Solids 23, 639 (1962).

11. M. Doyama and R. M. J. Cotterill, Lattice Defects and Their Interactions, R. R. Hasiguti, ed., Gordon and Breach, New York (1968).

12. L. Tewordt, Phys. Rev. 109, 61 (1958).

13. K. H. Bennemann, Z. Phys. 165, 445 (1961).

14. R. A. Johnson, Phys. Rev. 145, 423 (1966).

15. G. Borrman, Z. Phys. 127, 297 (1950).

16. B. W. Batterman and H. Cole, Rev. of Mod. Phys. 36, 681 (1964).

17. R. W. James, Solid State Physics, Vol. 15, p. 53, F. Seitz and D. Turnbull, eds., Academic Press, Inc., New York, (1963).

18. P. H. Dederichs, Phys. Cond. Materie 5, 347 (1966).

19. Y. H. Ohtsuki and S. Yanagawa, J. Phys. Soc. Japan 21, 326 (1966).

20. H. Wagenfeld, Phys. Rev. 144, 216 (1966).

21. Y. Shimomura, Phil. Mag. 19, 773 (1969).

22. Y. Shimomura, (to be published).

23. G. P. Scheidler and G. Roth, International Conference on Vacancies and Interstitials in Metals, p. 391, Kernforschungsanlage Jülich, West Germany (1968).

24. P. H. Dederichs, Phys. Stat. Sol. 23, 377 (1967).

25. P. H. Dederichs, (to be published).

26. F. W. Young, Jr., T. O. Baldwin and P. H. Dederichs, International Conference of Vacancies and Interstitials in Metals, Kernforschungsanlage Jülich, West Germany (1968), (to be published).

27. F. W. Young, Jr., and J. R. Savage, J. Appl. Phys. 35, 1917 (1964).

28. F. W. Young, Jr., and T. R. Wilson, Rev. Sci. Insts. 32, 559 (1961).

29. R. M. Nicklow, F. A. Sherrill, and F. W. Young, Jr., Phys. Rev. 137, A1417 (1965).

30. B. Okkerse and P. Penning, Phillips Res. Repts. 18, 82 (1963).

31. P. Penning and D. Polder, Phillips Res. Repts. 16, 419 (1961).

32. L. P. Hunter, J. Appl. Phys. 30, 874 (1958).

33. D. N. Batchelder and R. O. Simmons, J. Appl. Phys. 36, 2864 (1965).

34. J. E. Whitehouse, T. A. Callcott, J. A. Naber, and J. S. Raby, Rev. Sci. Instr. 36, 768 (1965).

35. P. B. Hirsch, Acta. Cryst. 5, 176 (1952).

36. O. S. Oen, Cross Sections for Atomic Displacements in Solids by Fast Electrons (ORNL-3813), (1965).

37. R. A. Johnson, J. Phys. Chem. Solids 28, 275 (1967).

38. A. C. Damask and G. J. Dienes, Point Defects in Metals, Gordon and Breach, eds., New York (1963).

39. K. C. Lie and J. S. Koehler, Adv. in Phys. 17, 421 (1968).

40. R. A. Johnson, J. Phys. Chem. Solids 26, 75 (1965).

41. T. O. Baldwin, F. W. Young, Jr., and A. Merlini, Phys. Rev. 163, 591 (1967).

42. F. Seitz and J. S. Koehler, Solid State Physics, Vol. 2, F. Seitz and D. Turnbull, eds., Academic Press, Inc., New York (1956).

43. R. A. Johnson, private communication, (1969).

VITA

Lewis Selig Edelheit was [redacted] and attended primary and secondary schools in that city.

He received a B.S. degree in Engineering Physics (with high honors) at the University of Illinois in June, 1964.

He entered the Graduate College, University of Illinois in September, 1964, and received an M.S. degree in Physics in February, 1966.

He held a teaching assistantship (1964-1965), a National Aeronautics and Space Administration Traineeship (1965-1968), and a E. I. Du Pont De Nemours Fellowship (1968-1969).

He is a member of the American Physical Society and Tau Beta Pi.